DIPLOMA THESIS
TITLE: Investigations of the complex impedance of Photovoltiac cells under illumination

July 21, 2011

Dedication

I dedicate this work to my parents Engr. & Mrs. Livinus O. Ebe who toiled to see my future dreams become a reality; my brothers and sisters: Constantine, Bruno, Emmanuel, Silverlin, Mary, Theresa, and Elizabeth. I dedicate this work to the entire Dominic Ebe's family especially to my uncles: Mr. S.N.D. Ebe, Nze. Patrick Ebe and Mr.Gerald Ebe.

Acknowledgment

I am grateful to Almighty God for His grace and sustenance all through this long academic journey.
I am grateful to my supervisor Ass. Prof. Dr. Viktor Schlosser for his paternal guidance and the moderation of this work as well as for his patience, encouragement and advice.
My profound gratitude goes to my cousin Rev. Fr. Sabinus Iweadighi whose guidance and instruction encouraged me to study hard. I will not hesitate to thank Rev. Fr. Cyril Nwakamma for his moral support and advice.
To my family members, I am indebted to you and I say thank you so much for your love and concern. In a special way, I am very grateful to my parents Engr. Livinus Ebe and Mrs. Imelda Ebe for my upbringing and their encouragement when the goings seemed unbearable. I thank my brothers Constanine, Bruno, Emmanuel and sisters Mrs. Silverline Ohuamalam, Mary, Theresa and Elizabeth for what they have been to me. I will not forget to express my profound gratitude to my family friends Hochstöger and Heneis for their assistance and encouragements during my academic studies. My special gratitude goes also to Pfr. Dechant Leopold Bösendorfer for his continuous encouragement and support. And to all who contributed immensely in one way or the other to the success of this work, I say thank you and God bless. May Almighty God reward you all abundantly.

Contents

1. Motivation

Photovoltaics is commonly known as the technological symbol for a future sustainable energy source in most countries. Due to the challenges faced by photovoltaic cells, a lot of money is already invested in research and development to improve their efficiency as well as material performance and to minimize their production cost [11]. The high and justified recognition of photovoltaics may be understood on the basis of the description of the main features which influence solar electric conversion [4].

Originally photovoltaic technology was commonly used in the power supply for off-grid professional applications and supply system (e.g. telecommunication gadget, solar home systems). More recently, the large-scale electricity generation as a substitute for other non-sustainable energy processes has become very important.

Photovoltaic energy conversion meets the necessary conditions of a sustainable energy production in an obvious way. The primary source of energy is the sun, during the conversion there exists no negative impact due to harmful emissions like CO_2 or waste (by-products). So solar electricity generation can also be called clean energy because it is “friendly” to the environment.

In recent times, there have been a lot of discussions on which other way energy could be used without harming the environment. Most developed countries use nuclear energy as a source for electricity generation which was then assumed to be more viable than any other conventional energy source. Now the opposite is the case, there have been several accidents occurring in nuclear power stations which may lead to massive destruction caused by radiative waste and emissions. The negative consequences of nuclear energy or other kinds of conventional energy has encouraged a lot of research on alternative energy resources (renewable energy).

Among the third world countries (Africa), poor power supply has been the major problem over the years due to insufficient energy sources. But today, the high intensity of the sun present in many regions of Africa has encouraged the use of photovoltaic cells to deliver the required energy. Every home will like to have solar panels instead of fossil energy source that cost a lot. The problem as well as the high cost of energy generation in Africa coupled with the high demand for renewable energy (solar electricity generation) motivated me to go into this research work on photovoltaic technology.

The aim of this thesis is to emphasize on the quality control during solar cell and module production which requires tools for a fast access to electrical parameters. That means the time of data acquisition preferably is below 1ms. In that case, both the real as well as the imaginary part of the impedance of the device have to be considered during data evaluation.

In a recent thesis Mrs. Kancsar has begun to investigate the AC behavior of solar cells [13]. At this time the general aspects have been elaborated. The present work was invoked due to the pending question in how far the results of the solar cell's complex impedance will effect the preferred fast transient recording of the electrical device parameters under operating conditions - in the forward voltage regime under illumination - for testing purposes.

2. Theory

The theory given below is a compendium focusing on the underlying principles of the present work. It is based on a literature search in different recognized text books [1-6, 8-10, 20, 27]. Newer results will be cited separately where necessary.

2.1. The physics of photovoltaic cells

A photovoltaic cell as an electrical power generator transforms the energy of incident radiation directly into electrical energy. The process of the energy conversion relies on the principles of quantum theory. Light is made up of packets of energy called photons, whose energy depends only upon the frequency or color of the light. The energy of one photon in the visible spectra is sufficient to excite one electron, bound in solids, up to higher energy levels where it is free to move [3].

2.1.1. Structure and operating principles

The technology of a photovoltaic device is generally based on the inner photoelectric or photovoltaic effect, which is responsible for the generation of free charges by photons as well as their movement within an internal electric field.

When a photon of sufficient energy is absorbed in the semiconducting material of the device, an electron is then excited from the valence band to the conduction band leaving behind a positively charged hole. This results into electron-hole pairs, which exist for a certain period before recombination occurs. The duration during which the electron-hole pair exists is called lifetime. In a solar cell, this electron-hole pair can be separated by an electric field which is usually recognized by a pn-junction. The electron-hole pair makes a statistical movement in a crystal, so there is a very high probability for the pair to enter the region where the carriers will be separated by the inner field, if the lifetime is sufficiently large. The separated charges develop a potential difference between both sides of the pn-junction,

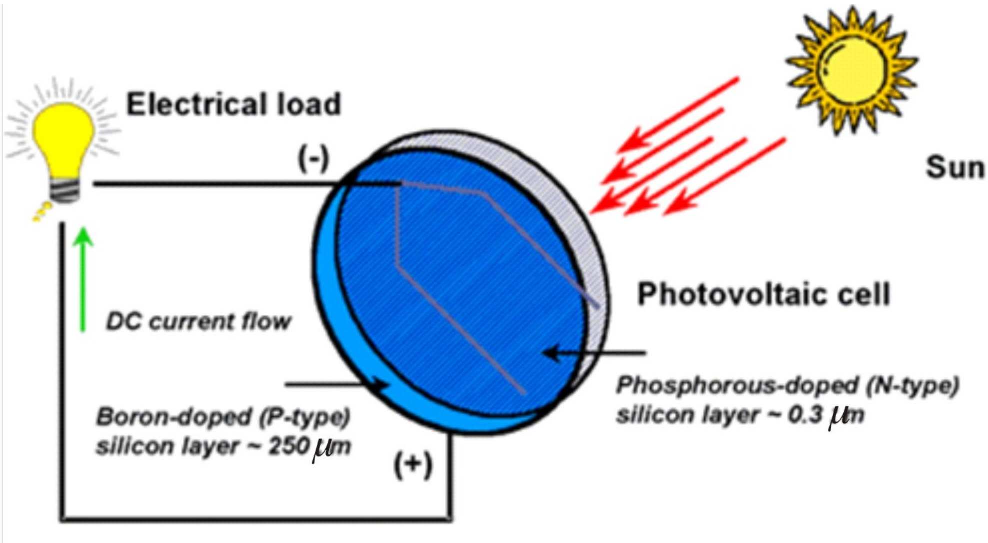

Figure 2.1.: The structure of a crystalline silicon solar cell and it's working principle (after [25])

which can be used to drive an external load as shown in Fig.2.1.

The number of generated electron-hole pairs is ideally equal to the number of photons with an energy greater than the gap energy. That means the light generated current directly depends on the intensity and spectral distribution of the incident light. Therefore, it is reasonable to describe the solar cell as a current generator associated with some internal loss mechanism. The cell characteristics can be described by the current-voltage relation (curve). Some important parameters can also be deduced from this relation, for instance, the open-circuit-voltage, the short-circuit current, the shunt resistance, the series resistance, the fill factor and others. More details can be found in [1,2, 3].

Fig. 2.1 shows the block diagram of a typical silicon solar cell, which is in use today. The electrical current generated in the semiconductor is extracted by the front and back contact of the cell. The top contact structure which allows light to pass through is made in the form of thin metal strips (usually known as fingers). The cell is coated with a thin layer of dielectric material called the "Anti reflection Coating" or ARC, which minimizes light reflection from the top surface.

2.2. The pn-junction

A pn-junction is the most commonly applied structure for charge separation in solar cells. It is formed when a p-type and a n-type semiconductor material are in direct contact with each other and form an interface as seen in Fig.2.2a. When these layers are brought together in direct contact, the holes diffuse from the p-type region into the n-type region and similarly, electrons from the n-type material diffuse into the p-type region due to their concentration differences in the two semiconductors. As the carriers diffuse, the charged impurities (ionized acceptors in p-type material and ionized donors in n-type material) are exposed -that is, no longer screened by the charges of the majority carriers. As long as these impurity charges are exposed, an electric field (or electrostatic potential difference) is established, which limits the diffusion of holes and electrons. In thermal equilibrium, the diffusion and drift currents for each carrier type is exactly balanced, so there is no net current flow. More over, in between the n-type and p-type materials, there exists a transition region called the Space-Charge Region, SCR, with respect to the ionized atoms in the semiconductor's lattice. It is also often called the depletion region for free carriers, and is depleted of both holes and electrons. Assuming that the p-type region and n-type regions are sufficiently thick, the regions on either side of the depletion region are essentially charge-neutral (often termed quasi-neutral). The electrostatic potential difference resulting from the junction formation is called the built-in voltage, U_{bi}. It arises from the electric field created by the exposure of the positive and negative charged space in the depletion region and is determined by the difference in the work functions of the p- and n-type materials, Φ_p and Φ_n. The difference in work functions is equal to the difference in the shift of the Fermi levels from the intrinsic potential energy of the semiconductor, since E_i is parallel to E_{vac}. Hence

$$U_{bi} = \frac{1}{q}(\Phi_n - \Phi_p) = \frac{1}{q}((E_i - E_F)|p_{side} - (E_i - E_F)|n_{side}). \tag{2.1}$$

[3]

In a typical silicon solar cell as shown in Fig.2.1., the p-type wafer forms the base of the cell, but is slightly doped to hinder recombination. The n-type layer of

the wafer is created by a dopant diffusion at one surface of the wafer. In contrast to the base this layer is heavily n-doped (n^+) in order to achieve the preferred step like transition. The concentration of the acceptors N_A in the p-region is about $10^{16}cm^{-3}$ while that of the donors N_D in the n-region is about $10^{19}cm^{-3}$. Due to high chances of recombination in the heavily doped n-type layer, it is favorable to make it as thin as possible [13] .
After the formation of the pn-junction, there exists a built-in potential. The magnitude of this potential depends on the gradient of impurity atoms in the semiconductor matrix. The built - in voltage U_{bi} of the junction in Equation 2.1 can also be expressed in terms of the doping concentrations N_D and N_A once all dopants are ionized as described by Equation 2.2 .

$$U_{bi} = \frac{K_B T}{q} \ln\left(\frac{N_D N_A}{n_i^2}\right) \tag{2.2}$$

Note, the Equation 2.2 do not show how U_{bi} depend on the gradient of the doping concentration! It is exactly valid only once the gradient is assumed to be a step function. This is the case for an abrupt pn-junction.

In thermal equilibrium, the intrinsic carrier concentration n_i is given by definition as [27]

$$n_o p_o = n_i^2 = N_c N_v e^{-\frac{E_g}{K_B T}} \tag{2.3}$$

n_i represents the concentration of electrons which are thermally excited into the conduction band of the intrinsic or undoped semiconductor, while n_o and p_o represents the equilibrium concentrations of electrons and holes in the doped material, N_c and N_v are material constants.
U_{bi} gives the an upper limit that can not be exceeded by the open circuit voltage U_{oc} of the solar cell [1, 3, 4].

2.2.1. The pn-junction under bias condition

To understand the operation of a solar cell, we need to understand what happens

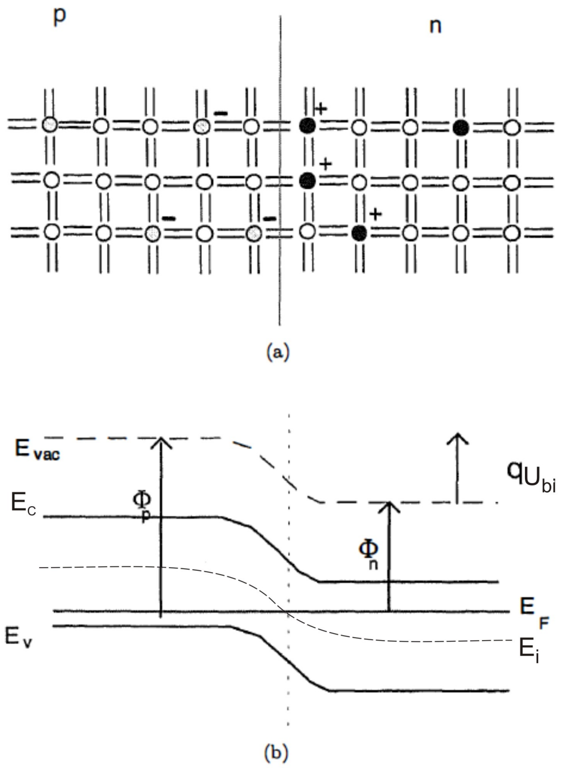

Figure 2.2.: (a) Schematic of the crystal structure close to a pn-junction including charged dopant atoms; (b) Energy profile across the junction in equilibrium (after [3]).

to the semiconductor device when it is displaced from it's thermal equilibrium state. The thermal equilibrium can be easily displaced either by an external bias voltage or by illumination.

More over, the understanding of the behavior of a pn-junction will also lead us to the understanding of the working principle of solar cells. The current flow in a pn-junction depends mostly on the polarity of the applied bias voltage as displayed in the current-voltage characteristics in Fig.5.1. When a forward bias voltage ($U > 0$) is applied to the device in the dark, the built in potential across the junction will decrease by a factor ($U_{bi} - U$). In this case, the built in potential for the majority carriers at the junction is reduced, and the width of the space charge or depletion region is reduced. The net diffusion current flow to the junction will increase exponentially with the increase of the applied voltage as described by Equation 2.4.

The dark diffusion current, I_{dark} of the device under applied bias voltage is equal to the sum of individual diffusion current contributions from the SCR (p-region and n-region) [3]. It is given by :

$$I_{dark} = I_p + I_{SCR} + I_n = I_o(e^{(\frac{qU}{nK_BT})} - 1) \tag{2.4}$$

where n represents the diode factor and I_o the saturation current.

Similarly, when a reverse bias voltage ($U < 0$) is applied to the junction, the built-in potential across the junction will increase to ($U_{bi} + U$). Therefore the built-in potential of the majority carriers across the junction will increase as well as the width of the depletion region with the increase of the reverse bias voltage. As a result, the current flow through the junction becomes very small due to the high impedance of the junction. The saturation current or reverse current is ideally a constant represented as -I_o. A very high reverse voltage however will result to a phenomena called reverse break down where the negative current increases rapidly again. This case is not described by Equation 2.4 and may lead to the irreversible destruction of the pn-junction. The operation condition of photovoltaic cells for power delivering always is in the forward bias range, $0 < U < U_{bi}$ [12, 13].

Equation 2.4 applies for both :

(a) forward bias voltages, when $U > 0$, $e^{\frac{qU}{nK_BT}} \gg 1$

(b) not too large reverse bias voltages, when $U < 0$, $e^{\frac{qU}{nK_BT}} \ll 1 \rightarrow$ then $I_{dark} \approx -I_o \ldots\ldots\ldots$ saturation current

When the solar cell is illuminated, photon absorption will take place. The absorbed photon excites an electron-hole pair which contributes to an additional current (photo-current, I_{ph}). It is also known as the light generated current. The actual net current of the cell is then :

$$I = I_{dark} - I_{ph} \tag{2.5}$$

The electric power delivered by the cell is defined as the the product of the net

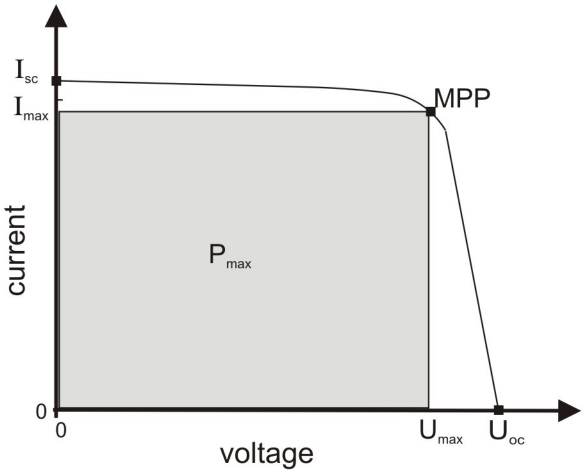

Figure 2.3.: A typical current-voltage curve for a solar cell

current and the bias voltage and is given by :

$$P = I \cdot U \tag{2.6}$$

We can also estimate or evaluate the maximum power P_{max} delivered by the cell to the external load from a point along the current-voltage characteristics called maximum power point (MPP) as illustrated in Fig.2.3:

$$P_{max} = I_{max} \cdot U_{max} \tag{2.7}$$

Fig.2.3 shows the current voltage characteristics, $I(U)$ of a solar cell. The short circuit current is given by I_{sc} and the open circuit voltage voltage by U_{oc}. At $P = P_{max}$ the voltage $U_{max}$is slightly less than U_{oc} whereas for highly efficient cells the current maximum remains close to the short circuit current $I_{max} \simeq I_{sc}$.

Under illumination, cell parameters like I_{sc}, and U_{oc} of a photovoltaic cell can be calculated or derived from the $I(U)$ characteristics:

$$U_{oc} = U_T \ln \left(\frac{I_{ph}}{I_o} + 1 \right) \tag{2.8}$$

where it is assumed that $I_{sc} \simeq I_{ph} \gg I_0$. Equation 2.8 is a consequence of Equation 2.4 for the case that $I = 0 = I_{dark} - I_{ph}$ where the exponent's argument is simplified to$U_T = \frac{qU}{nK_BT}$

2.3. The equivalent circuit model of a solar cell

Since semiconductor physics merely gives an ideal view of the solar cell, it is necessary to extend it with respect to the electric behavior of real devices.

To understand the electronic behavior of a solar cell in more detail, it is very convenient to create an equivalent circuit model which is composed of discrete electrical elements as a basic tool. Solar cells can be regarded as an ideal DC current generator with several internal losses. The produced DC current is linearly proportional to the incident light intensity. We can use several types of DC models for the photovoltaic cells. The core DC model consists of a current source in parallel with a single semiconductor pn-junction diode. The most common model used for the analysis of the crystalline silicon cell's behavior is a double diode model. The double diode DC model accounts for both the diffusion and recombination phenomenon that occurred for this kind of cells. Most often this circuit is extended by two passive resistors accounting for shunt and series effects.

2.3.1. The DC model

In the DC equivalent circuit a typical photovoltaic cell is modeled by a current source in parallel with a pn-junction diode as shown in Fig.2.4. Moreover, an ideal photovoltaic cell can be modeled electrically equivalent to a current generator, producing a photo current into the electric circuit, in parallel with a diode.

In practice, no photovoltaic cell is ideal and it's DC equivalent circuit therefore is modeled with an additional parallel shunt resistance and a series resistance which are regarded as *parasitic resistance*s. Among these parasitic resistances, each may

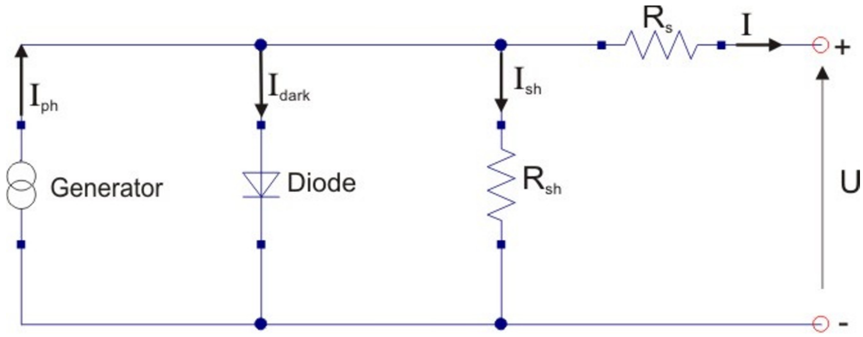

Figure 2.4.: One diode equivalent circuit model of a solar cell

contribute to the non ideal characteristics of the cell. The series resistance R_s is, however, the most common problem in practical photovoltaic cells. It results from the bulk resistance of the p- and n-layer to majority carriers flow as well as from the ohmic contacts on the cell to the external wiring. The effect leads to a potential drop of $I \times R_s$ between the junction and the external applied voltage U. The difference between U at the terminals and the voltage U' is given by Equation 2.9 [3].

$$U' = U - IR_s \tag{2.9}$$

where IR_s is the voltage drop due to the series resistance. U' is the voltage that is "seen" by the "ideal" diode.

The parallel or shunt resistance R_{sh} results primarily from the leakage currents around the edges of the photovoltaic cell or the poor insulation at both terminals of the photovoltaic cell and inhomogeneities due to defects encountered during production. In order to obtain maximum efficiency of the PV-cell, the series resistance should be small , while the parallel resistance should be as large as possible.

Fig.2.4 represents the DC equivalent circuit model with a single diode and the two parasitic resistances.

The net current flow through the device under illumination is given by the relation:

$$I = I_{dark} + I_{sh} - I_{ph} \tag{2.10}$$

Equation 2.10 is then transformed to give the general form for the current-voltage characteristic by a combination of Equation 2.4 and 2.9. That is :

$$I = I_o(e^{\frac{q(U-IR_s)}{nK_BT}} - 1) + \frac{U - IR_s}{R_{sh}} - I_{ph} \tag{2.11}$$

According to some literature [3, 4] the sign convention for the photo current, I_{ph} is often positive in the first quadrant of the coordinate along the current-voltage curve, such that the power out put of the cell is positively defined. In this work, the usual convention for semiconductor electronic devices is maintained and will be used for further circuit model analysis as seen in Equation 2.10.

We have to note, that all the parameters of PV cells depend on their physical geometry likewise on the size or area A of the cells. Such parameters like I_o, R_{sh}, R_s, and I_{ph} will be assigned values per unit area ($1cm^2$) as expressed by Equation 2.12:

$$J = \frac{I}{A} = J_o\left(e^{\frac{q(U-Jr_s)}{nK_BT}} - 1\right) + \frac{U - Jr_s}{r_{sh}} - J_{ph} \tag{2.12}$$

A substitution of Equation 2.9 into Equation 2.12 finally result in:

$$J(U) = J_o\left(e^{\frac{qU^{'}}{nK_BT}} - 1\right) + g_{sh}U^{'} - J_{ph} \tag{2.13}$$

(Current-voltage characteristic general form).

where ,

J	current density	Acm^{-2}

J_o	saturation current density	Acm^{-2}
J_{ph}	photo current density	Acm^{-2}
U'	diode voltage	V
$r_s = (R_s A^{-1})$	area normalized value of series resistance	Ωcm^{-2}
$r_{sh} = (R_{sh} A^{-1})$	area normalized value of shunt resistance	Ωcm^{-2}
$g_s = (r_{sh} A)^{-1}$or $(G_{sh} A^{-1})$	area normalized value of shunt conductance	Scm^{-2}

Several mechanisms contribute to the diode current. Using a single diode model makes it necessary to adapt the magnitude of the diode factor n to best match the experimental current voltage characteristics.
At a given bias voltage, usually only one effect dominates the current-voltage characteristics. In this case however where you want to characterize the cell over a wide bias range, it is preferable to introduce several diodes with different diode factors and saturation currents. For a crystalline silicon (c-Si) cell operated at room temperature, there are mainly two mechanisms which contribute to the resulting diode current: recombination and diffusion. The first term is dominant for small bias voltages ($U \lesssim +0.3V$) while the second at higher voltages ($V > +0.5V$). Therefore, sometimes a two diode model is introduced as illustrated in Equation 2.14.

$$I = I_{01}\left(e^{\frac{q(U-IR_s)}{K_BT}} - 1\right) + I_{02}\left(e^{\frac{q(U-IR_s)}{2K_BT}} - 1\right) + \frac{U-IR_s}{R_{sh}} - I_{ph} \tag{2.14}$$

Where the first diode describes the diffusion current I_{diff} and is given by:

$$I_{diff} = I_{01}\left(e^{\frac{q(U-IR_s)}{K_BT})} - 1\right) \tag{2.15}$$

The second term of Equation 2.14 represents the recombination current I_{rec}:

$$I_{rec} = I_{02}\left(e^{\frac{q(U-IR_s)}{2K_BT}} - 1\right) \tag{2.16}$$

and I_{01} and I_{02} are constants assumed to be voltage independent. However they strongly vary with temperature.

Among these constants, I_{01} represents the diffusion saturation current, while I_{02} represents the recombination saturation current. Depending on the dominant mechanism $n = 1$ takes care of the diffusion current and $n = 2$ for recombination current.
[5, 22, and 23]

2.3.2. The AC model

Similar to the DC model, the AC equivalent circuit generally consists of a current generating source that initiate the photo current into the electric circuit as illustrated in Fig.2.5. The DC model is, however, extended by two capacitors C_T and C_d in parallel and an inductance L_{grid} in series to R_s. The sum of the two capacitors (the transition capacitance C_T and the diffusion capacitance C_d) contributes to the total capacitance C_J of the pn-junction as described in detail in section 2.3.2.2 of this work. The inductance L_{grid} originates from the front contact metal finger grid and is considered to be voltage as well as frequency independent.
Following the approach of Millman and Halkias, a cell resistance R_P is defined as the parallel combination of the static, R_T and the dynamic, R_d resistance. These resistances are determined or evaluated from current-voltage characteristics as given in Equation 2.11. Among all the AC parameters of the cell, the most important is it's parallel resistance R_P [9].

The static resistance is given by [9]

$$R_T = \frac{U}{I} \tag{2.17}$$

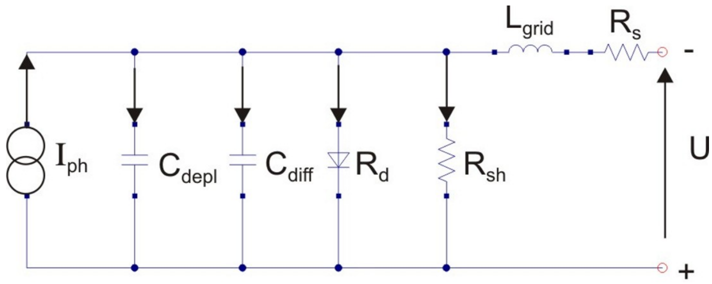

Figure 2.5.: AC circuit model of a crystalline silicon solar cell

The dynamic resistance R_d is evaluated from the current-voltage characteristic from Equation 2.11 above and is given as :

$$R_d = \frac{1}{dI/dU}. \tag{2.18}$$

[9]

The effective or parallel resistance of a PV cell is then given by Equation 2.19

$$R_P = \frac{R_T R_d}{R_T + R_d}. \tag{2.19}$$

The Complex Impedance

The AC equivalent circuit model of the device in Fig.2.5 has three non ohmic components, namely the capacitors C_{depl} and C_{diff} as well as an inductor L_{grid} which causes the complex impedance once I_{ph} contains an AC current component. The complex impedance Z consists of a real and an imaginary part :

$$Z = \frac{U_{AC}}{I_{AC}} = R + iX = \mid Z \mid e^{i\varphi} \tag{2.20}$$

Here R expresses the real part of the impedance whereas iX represents the imaginary part as indicated by the symbol of the imaginary unit i. The later is originated from the non ohmic components: the capacitance and the inductance in the circuit. These two elements cause a phase difference between current, I_{AC} and voltage, V_{AC}.

A capacitor bears a pure reactive impedance which varies inversely proportional to the signal frequency and the magnitude of the capacitance. The capacitive reactance, X_C is given by :

$$X_C = \frac{-1}{\omega C} \tag{2.21}$$

Where , $\omega = 2\pi f$ is the angular frequency of an AC signal input. Thus the decrease in X_C results from increase in signal frequency as well as the magnitude of the capacitor .

The inductance or inductive reactance is also given by :

$$X_L = \omega L \tag{2.22}$$

Therefore, the net reactance is given by :

$$X = X_L + X_C = \omega L - \frac{1}{\omega C} \tag{2.23}$$

In opposite to the capacitor, the inductive reactance of an inductor varies directly proportional to the signal frequency as well as to the magnitude of an inductor.

The complex impedance can also be represented as a vector in the complex plane form and it's absolute value or amplitude is given by :

$$\mid Z \mid = \sqrt{R^2 + \left(\omega L - \frac{1}{\omega C}\right)^2} \tag{2.24}$$

And the phase displacement between the alternating current, I_{AC} and the voltage, U_{AC} is given by :

$$\varphi = \arctan(\frac{Im\{Z\}}{Re\{Z\}}) = \arctan\left(\frac{\omega L - \frac{1}{\omega C}}{R}\right) \tag{2.25}$$

[20]

Junction capacitance

The capacitance of a photovoltaic device originates from the pn-junction and is generally, the sum of two voltage dependent components namely: the depletion capacitance, C_{depl} and the diffusion capacitance, C_{diff}. A description of the origin of each of these capacitance components will be treated separately depending on the bias regime of the pn-junction.

The depletion capacitance arises from the variation in the width of the depletion region in the pn-junction. Such effect arises, if the device is operated in the reverse bias regime and the junction capacitance approximately equals to depletion capacitance. In this case, it can be said that, the pn-junction diode becomes functionally a voltage dependent capacitor in the reverse bias regime.

In this case the junction capacitance is concluded in analogy to a parallel plate capacitor. The capacitance of a parallel plate capacitor, C_J is given by:

$$C_J = \frac{\epsilon_s \epsilon_o A}{W} \tag{2.26}$$

Where, A is the area of the (equally sized) plates , W is the distance between the two plates and ϵ_s is the dielectric constant of the dielectric material between the plates. In the pn-junction, A is the area of the pn-junction plane and W is the width of the depletion region. ϵ_s is the dielectric constant of the semiconductor. The major difference is that the pn-junction exhibits a continuous charge distribution inside the depletion region whereas in the plate capacitor, the charges are fully separated by the distance W and no charges are present between the plates.

For a pn-junction the width W of the depletion region is given by:

$$W = \sqrt{\frac{2\epsilon_s\epsilon_o}{q}\left(\frac{N_A + N_D}{N_A N_D}\right)(U_{bi} - U)} \tag{2.27}$$

For the step like doping profile, where $N_D \gg N_A$ Equation 2.27 simplifies to

$$W = \sqrt{\frac{2\epsilon_s\epsilon_o}{q}\left(\frac{1}{N_A}\right)(U_{bi} - U)} \tag{2.28}$$

[5]

This is frequently fulfilled for c-Si solar cells (section. 2.2, $N_A \sim 10^{16}cm^{-3}$, $N_D \sim 10^{19}cm^{-3}$)

With Equations 2.26 and 2.28 the depletion capacitance, C_{depl} can be rewritten:

$$C_{depl} = A\sqrt{\frac{q\epsilon_s\epsilon_o N_A}{2\,(U_{bi} - U)}} \tag{2.29}$$

[9]

The depletion capacitance as defined by Equation 2.29 varies only with voltage but doesn't depend on the frequency.

On the other hand, when the pn-junction diode is forward biased, the depletion region decreases and an additional contribution to the junction capacitance appears, which aroused from the rearrangement of the minority carriers injected into the quasi-neutral region. This contribution is called the diffusion capacitance, C_{diff}.

In this case, the width of the depletion region appears to diminish and the depletion capacitance at the same time becomes negligible, that is, $C_{depl} \ll C_{diff}$ [7] .

The approximation for the diffusion capacitance is given by Equations 2.30 and 2.31 as follows:

$$C_{diff} = \frac{\tau q}{2k_B n} I_o e^{(qU/nK_B T)} \tag{2.30}$$

for low frequencies ($\omega\tau \ll 1$) and

$$C_{diff} = \left(\frac{\tau}{2\omega}\right)^{\frac{1}{2}} \frac{q}{k_B n} I_o e^{(qU/nK_B T)} \tag{2.31}$$

for very high frequencies ($\omega\tau \gg 1$) [9]
where,τ is the minority carrier life time . As it can be seen from 2.30 and 2.31, the diffusion capacitance depends on the voltage and on the frequency.

In the above expression, the exponential term; $I_o e^{(qU/nK_B T)}$ is approximately the forward current across the junction. For a crystalline silicon solar device at room temperature the recombination current dominates the pn-junction behavior for $U < 0.3V$, (see section 2.3.1). Here the voltage dependence will be proportional to $e^{(qU/2K_B T)}$.

Small Signal Model

In this section, we examine the small signal response of a pn-junction diode with the aid of a common analysis technique the so called *small signal model.* This technique is used to approximate the behavior of nonlinear devices through the linearization of the current-voltage equations around a DC voltage working point. In addition, the piecewise linear approximation of the exponential diode characteristic could also be achieved either from the graphical approach as illustrated in Fig.2.6 or mathematically. The mathematical approach will only emphasized on the linear approximation of the diode characteristics, which will lead us to the

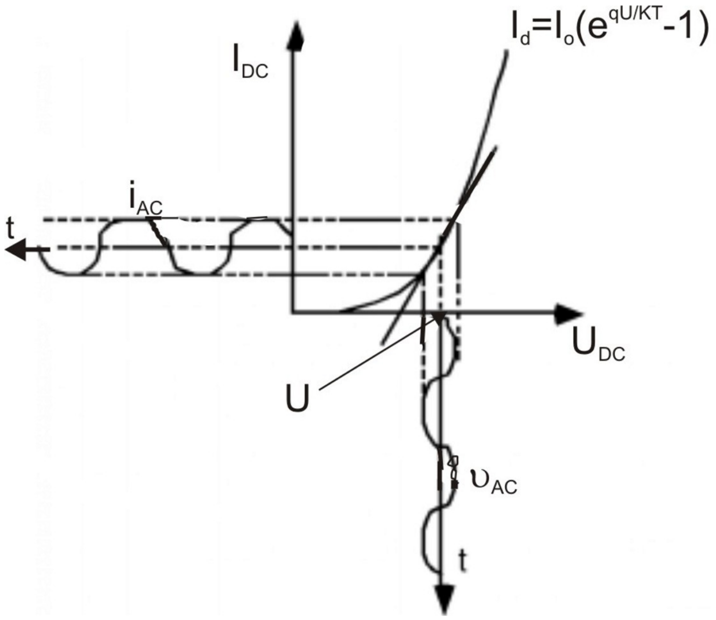

Figure 2.6.: Graphical representation of the small signal response of a pn-junction device.

derivation of AC response of the pn-junction device.

Mathematically the piecewise linear approximation of the diode Equation 2.4 corresponds to the first derivative of this function and can be used to evaluate the diffusion capacitance, C_{diff} and the differential conductance, G_{AC} of a forward biased pn-junction diode.

We consider the response of a c-Si pn-junction photovoltaic cell to a small AC voltage, υ_{AC} of the signal's angular frequency, ω superimposing an applied DC voltage U_{DC}. This could be considered a disturbance from the operating point introduced by the current, I through the device and the applied bias voltage U_{DC} will occur. In order to achieve a good result, a linear relationship between current and voltage has to be found around a bias point which should be used for the signal analysis. The linear approximation applied for a given small disturbance υ_{AC} leads to the establishment of the small signal admittance equivalent circuit in Fig.2.7. The AC response of a pn-junction diode is generally characterized by the small signal admittance $Y = i_{AC}/\upsilon_{AC}$, which is derived mathematically in detail.

The overall voltage in the circuit is given by Equation 2.32

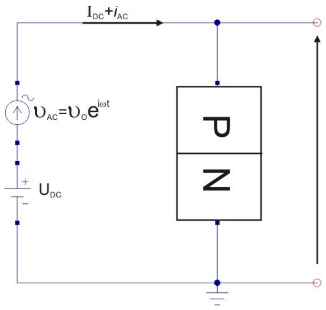

Figure 2.7.: Small signal equivalent circuit model of a pn-junction diode.

$$U(t) = U_{DC} + v_{AC} = U_{DC} + v_o e^{i\omega t} \tag{2.32}$$

By definition, we assume $v_o \ll U_{DC}$ and $U_{DC} > 0$ (forward biased).

The overall current flowing through the junction of the device, $I(t)$ will now contain the AC component i_{AC} as written in Equation 2.33:

$$I(t) = I_{DC} + i_{AC} = I_{DC} + i_o e^{(i\omega t - \varphi)} \tag{2.33}$$

Again we assume $i_o \ll I_{DC}$

Consider a case where there is no signal introduced in the circuit, that is, $v_{AC} = 0$. Then the overall current becomes I_{DC} as in the diode characteristic of Equation 2.4, that is,

$$I = I_{DC} = I_o(e^{\frac{qU}{K_B T}} - 1) \approx I_o e^{\frac{qU}{K_B T}} \tag{2.34}$$
$$\text{for} \quad e^{\frac{qU}{K_B T}} \gg 1$$

From Equation 2.34, the differential conductance of a pn-junction diode is then evaluated as the derivative of the current-voltage characteristic at DC voltage bias as illustrated in Fig.2.6 and is given by:

$$G_o = \frac{\Delta I_{DC}}{\Delta U_{DC}} = \frac{dI_{DC}}{dU} |_{U=U_{DC}} = I_o \frac{q}{k_B T} e^{\frac{qU_{DC}}{K_B T}} \tag{2.35}$$

Equation 2.35 is common for every diode operating in the forward bias regime, but the conductance tends to zero (vanish) in the case of reverse bias.

When a small signal is introduced superimposing the DC bias, the total voltage becomes the sum of U_{DC} and v_{AC} as seen in Equation 2.32. Then the differential conductance of the junction in the presence of the small AC signal is given :

$$G_{AC} = \frac{dI(t)}{dU(t)} \tag{2.36}$$

Considering the bulk properties of the planar pn-junction, the differential conductance G_{AC} derived from small signal measurement is expected to be equal to the first order derivative of the diode characteristic given by Equation 2.35. Hence :

$$G_{AC} \approx G_o \tag{2.37}$$

From 2.32 we substitute for $U : U + v_{AC}$

Thus, the current flowing through the device will now be :

$$I(t) = I_{DC} + i_{AC} = I_o(e^{\frac{qU}{K_B T}} - 1) = I_o(e^{\frac{q(U_{DC}+v_{AC})}{K_B T}} - 1) \approx I_o e^{\frac{q(U_{DC}+v_{AC})}{K_B T}} \tag{2.38}$$

We note that ,

$$e^{\frac{q(U_{DC}+v_{AC})}{K_B T}} = e^{\frac{qU_{DC}}{K_B T}} \cdot e^{\frac{qv_{AC}}{K_B T}} \tag{2.39}$$

For $qv_{AC} \ll k_BT$, power series expansion can be applied:

$$e^{\frac{qv_{AC}}{K_BT}} \approx 1 + \frac{qv_{AC}}{K_BT} + \cdots \tag{2.40}$$

With respect to the first order Equation 2.34, is rewritten as

$$I_{DC} + i_{AC} = I_o e^{\frac{qU_{DC}}{K_BT}} \left(1 + \frac{qv_{AC}}{K_BT}\right) \tag{2.41}$$

Obviously, the first term of Equation 2.41 accounts for the DC component as defined by Equation 2.34

$$I_{DC} = I_o e^{\frac{qU}{K_BT}} \tag{2.42}$$

thus i_{AC} is given by:

$$i_{AC} = \frac{qv_{AC}}{K_BT} I_{DC} \tag{2.43}$$

Then we have that ,

$$\frac{i_{AC}}{v_{AC}} = \frac{q}{K_BT} I_o e^{\frac{qU}{K_BT}} = G_{AC} = Y \tag{2.44}$$

which is equal to Equation 2.35.$G_{AC} = G_o$

The small signal admittance generally consists of a real and an imaginary part introduced by the applied small AC voltage amplitude. The total admittance is then given by :

$$Y = G_0 + iB \tag{2.45}$$

where B is the susceptance and can also be deduced from the diffusion capacitance as given in Equation 2.46

$$B = \omega C_{diff} \tag{2.46}$$

The analysis of the small signal admittance of a pn-junction device with $N_D \gg N_A$is finally given by :

$$Y = G_o\sqrt{1 + i\omega\tau_{SCR}} \tag{2.47}$$

where τ_{SCR} is the electron's life time in the space charge region and regarded as material constant. For $\omega\tau_{SCR} \ll 1$, the admittance Y is then approximated by series expansion to be:

$$Y \approx G_o\left(1 + \frac{j\omega\tau_{SCR}}{2}\right) \tag{2.48}$$

The conductance is then regarded as the diffusion conductance G_{diff} of a forward biased pn-junction and is given theoretically by :

$$G_{diff} = \frac{dI}{dU} = I_o\frac{q}{K_BT}\,e^{\left(\frac{qU}{nK_BT}\right)} \tag{2.49}$$

For the ideality factor $n = 1$, Equation 2.49 equals Equation 2.44 and Equation 2.35.
The diffusion capacitance in Equation 2.30 is finally expressed in terms of the conductance and the minority carrier life time from Equation 2.48 and is written as :

$$C_{diff} = \frac{G_{diff}\tau_{SCR}}{2} \tag{2.50}$$

A more complete evaluation of the small signal admittance of a pn-junction can be found in the following [5, 6, 8 and 21]

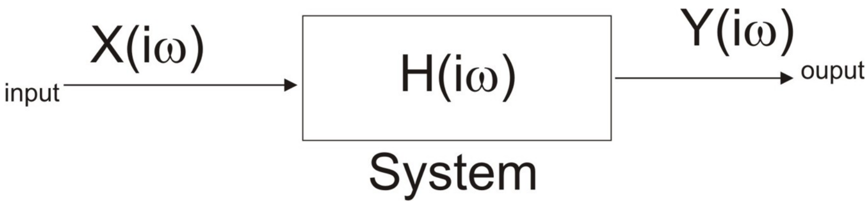

Figure 2.8.: Frequency response function.

The signal response function

The Response function (or frequency response) is generally defined as a quantitative measure of any system's output spectrum in response to an input signal. In general, a system responds differently to inputs at different frequencies. Some of them may have the ability to amplify components of certain frequencies, and to attenuate components of other frequencies.

The frequency response can also be called "Frequency Response Function" (FRF), which is the relationship between the system input and output in the Fourier domain as illustrated in Fig.2.8.

In this system, $X(i\omega)$ represents system input, $Y(i\omega)$ also represents system output and $H(i\omega)$ is the signal response (frequency response). The relationship between these functions is given by :

$$\frac{Y(i\omega)}{X(i\omega)} = H(i\omega) \tag{2.51}$$

According to Equation 2.51, the response is a complex function and it can be converted to polar notation in the complex plane.
We consider the case of a low pass filter characteristic as an example of the signal or frequency response, as illustrated in Fig.2.9 below. The term "Low Pass Filter", is generally defined as a filter that passes or allows low frequency signal outputs but attenuates the amplitude of signals with frequencies higher than the cut off frequency.

The resistance R and capacitance C in the electric circuit form a low pass filter which determine the cutoff frequency of a signal. The cut off frequency is given by :

$$f_{RC} = \frac{1}{2\pi RC} \tag{2.52}$$

The cut off frequency f_{RC} is the frequency at which the system's power output, P_{out} is attenuated to half the value of its power input, P_{in}:

$$P_{out} = \frac{1}{2} P_{in} \tag{2.53}$$

On the generally accepted logarithmic scale Equation 2.53 is expressed as power gain, G_P:

$$G_P = 10 \log \left(\frac{P_{out}}{P_{in}} \right) = 10 \log \left(\frac{1}{2} \right) = -3dB \tag{2.54}$$

with $P = \frac{U^2}{R}$ and $P = I^2 R$, Equation 2.54 can be expressed in terms of voltage or current, thus producing the voltage or current attenuation through the low-pass filter, then we have that :

$$G_U = 10 \log \left(\frac{U_{out}^2}{U_{in}^2} \right) = 20 \log \left(\frac{U_{out}}{U_{in}} \right) = -3dB \tag{2.55}$$

$$G_I = 10 \log \left(\frac{I_{out}^2}{I_{in}^2} \right) = 20 \log \left(\frac{I_{out}}{I_{in}} \right) = -3dB \tag{2.56}$$

in other words:

$$U_{out} = \frac{1}{\sqrt{2}} U_{in} \tag{2.57}$$

$$I_{out} = \frac{1}{\sqrt{2}} I_{in} \tag{2.58}$$

Considering Equation 2.25 in the previous section (2.3.2.1), the phase displacement φ between the input and output signal through the RC circuit is limited to $0 \leq \varphi \leq \frac{\pi}{2}$. The phase displacement corresponding to the cut off frequency is given by :

$$\mid \Delta\varphi \mid = \frac{\pi}{4} \tag{2.59}$$

With a low-pass filter RC current divider or voltage divider, the input-output current, as well as the input-output voltage relation can be achieved. The relations are given by:

$$I_{out} = \frac{\frac{1}{i\omega C}}{R + \frac{1}{i\omega C}} I_{in} = \frac{1}{1 + i\omega CR} I_{in} \tag{2.60}$$

Similarly,

$$U_{out} = \frac{1}{1 + i\omega CR} U_{in} \tag{2.61}$$

Finally, the relative amplitude, the phase displacement φ between I_{in}& I_{out} as well as U_{in}& U_{out} are given by the following equations:

$$\mid \frac{I_{out}}{I_{in}} \mid = \frac{1}{\sqrt{1 + (\omega RC)^2}} \tag{2.62}$$

$$\mid \frac{U_{out}}{U_{in}} \mid = \frac{1}{\sqrt{1 + (\omega RC)^2}} \tag{2.63}$$

$$\varphi = \arctan\left(\frac{-1}{\omega RC}\right) \tag{2.64}$$

[20 and 24]

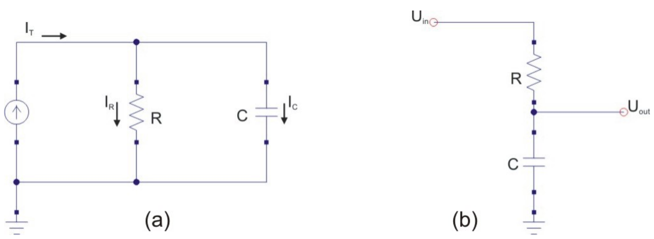

Figure 2.9.: (a) represents a low pass current divider, while (b) represents a low pass voltage divider.

3. Experimental setup

In this work, the small signal model technique was used to study the AC characteristic (the complex impedance) of a photovoltaic cell. The setup is basically equipped with a dual phase Lock in amplifier, a function generator, a digital storage oscilloscope, a power amplifier, a digital multimeter with an input matrix scanner, the photovoltaic cell is the device under test, DUT.

In addition, other elements like a temperature sensor (LM35) and a light intensity sensor (TSL50R) were mounted together with the DUT on a circuit board in order to monitor ambient conditions. A low voltage halogen lamp serves as a white light source to illuminate the DUT.

Before the experimental exercise, the above mentioned instruments were connected via GPIB interface to a PC and controlled by the National Instruments software "Lab Windows CVI". Indeed, programs were designed in such a way, that the measurement processes can be done automatically.
However, four different measurements were done on the DUT separately with different setups and each was repeated in the dark as well as under several illumination intensities. The dark measurement serves as a reference.

3.1. Instruments

3.1.1. Function generator

The function generator used in this work served as a signal generating device for both the small signal experiments as well as the frequency response measurements. The device is the type: Agilent Technologies 33220A Function/Arbitrary wave form generator that has a frequency range for sinusoidal waves from 1μHz to 20MHz. It's maximum harmonic distortion is -3dB_C.

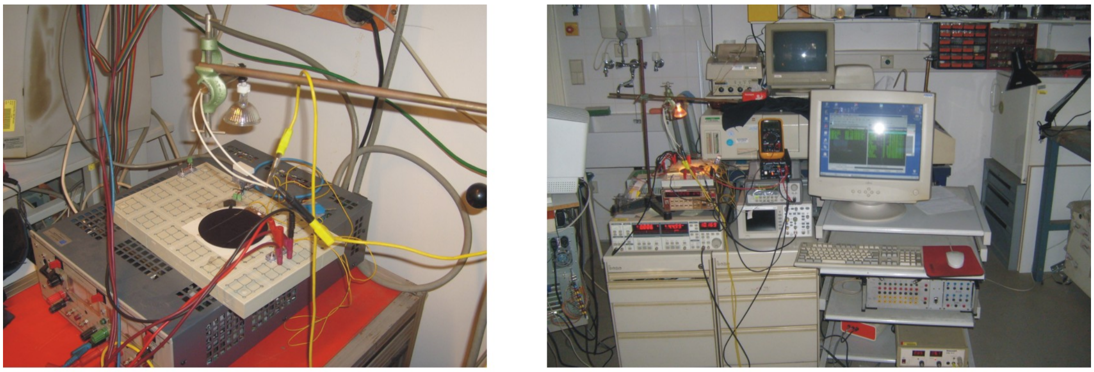

(a) (b)

Figure 3.1.: Images of the measurement setup:
(a) shows the building/testing of the setup while (b) shows the complete setup for all measurements.

3.1.2. Lock in amplifier

The Lock-in amplifier used, is the Stanford Instruments SR830 dual phase digital lock-in amplifier, which serves as frequency and phase sensitive voltage sensing device for the received signal. It is operated by two input channels, they are: the signal channel and the reference channel. The latter is connected to the trigger output of the function generator.
The signal channel has a selectable full scale sensitivity from $2nV$ to $1V$ with a typical maximum noise input of $6nV/\sqrt{Hz}$ at $1kHz$. It also bears line filters for $50Hz$ and $100Hz$. The second channel (reference channel) can be operated from external sources or from an internal sine wave generator. The specifications are as follows: frequency range from $1mHz$ to $120kHz$ at distortion of $-80dB_C$ and has a phase resolution of 0.01^o. The maximum amplitude it can bear is $5V_{rms}$ at a stability of $50ppm/^oC$. This built-in waveform generator however was never used in our experiments.
Simply, the lock in amplifier was used to detect and measure very small AC signals by means of amplitude and phase relative to the reference signal. Measurements could be made accurately even when the signal is obstructed by noisy sources many thousands of times larger than the signal.
Lock in amplifier, moreover, uses a technique of “phase-sensitivity detection” to

single out the component of the signal at a specific reference and phase. Noise signals at frequencies not equal to the reference frequency are rejected and do not disturb the measurement.

3.1.3. Oscilloscope

In the experimental exercise, the data acquisition was either done with a lock in amplifier or alternatively with a digital storage oscilloscope, DSO model Agilent DSO3062A. The instrument is specified by the manufacturer to have an analogue band width of $60MHz$, a vertical sensitivity ranging from $2mV/div$ to $5V/div$, and a horizontal sensitivity of $2ns/div$ to $50s/div$.
The Agilent DSO3062A has two channels, which have in common a real time sample rate of $1GSa/s$. On the two channels, measurements of the time-domain signal can be stored, each bearing a real time sampling rate up to $500MSa/s$. The term "sampling rate" is generally defined as the number of sample per second taken from a continuous signal to make a discrete signal.
For visual control of the signal's integrity or in the presence of a huge DC signal superimposing the AC component the DSO was preferred over the lock in amplifier.

3.1.4. Digital multimeter with scanner (DMMS)

The primary function of the device was it's built in switch capability between several input channels (Scanner Function). Besides it serves as DC voltmeter for auxiliary signals like Temperature and light intensity.

Some measurements like, DC current and DC voltage, resistance etc were taken by the digital multimeter scanner. The DMM scanner used, is Keithley Model 199. The instrument is a five function auto ranging digital multimeter. At 5½digit resolution, the LED display can display ±302.999 counts. The scanner option allows up to 8 two-terminal input sources to be connected. The DMM scanner has also a built in IEEE-488 interface, that makes it fully programmable over the IEEE-488 bus. The model 199 can make the following basic measurements and they are:

(1) DC voltage measurements from $1\mu V$ to $300V$

(2) Resistance measurements from $1m\Omega$ to $300M\Omega$

(3) TRMS AC voltage measurements from $1\mu V$ to $300V$

(4) DC current measurements from $1nA$ to $3A$

(5) TRMS AC current measurement from $100nA$ to $3A$

In our experiments only the DC voltage function was used.

3.1.5. Power amplifier

The signal of the function generator was amplified by the power amplifier in order to match the low impedance of the circuit. The device is already rated with maximum values of 13.8V and 3A.

3.2. Measurements

On the sample or DUT different experiments were carried out in the dark and under illumination. The purpose and conditions of the experiments are described in detail below.

3.2.1. DC Current-Voltage Measurement

In the dark, DC current-voltage measurements of the cell were done at ambient temperature (305.7K) under DC voltage bias ranged from -2.0V to +1.0V. On the same bias range, the same measurements were repeated for several intensities of the incident white light.

In the work, the current, I_{DC}, voltage, V_{DC} data pairs from the measurements were fitted with a two diode model with a least square fit routine. The results were used to determine the diode parameters as well as parasitic resistances namely R_s and R_{sh} and the solar cell parameters. The experimental setup for the DC current-voltage measurements is illustrated in Fig.3.2.

3.2.2. Small signal admittance measurement

Generally, admittance is defined as the inverse of the complex impedance as stated in Equation 2.48 (see section.2.3.2.2). In this experiment, emphasis is led only on

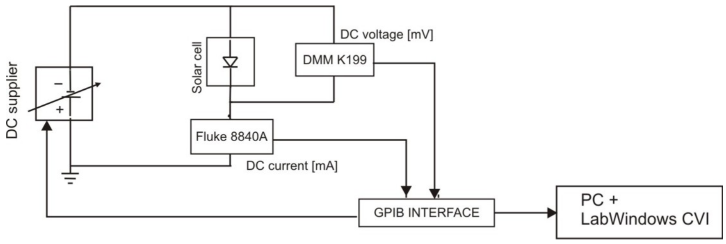

Figure 3.2.: Experimental setup for DC measurements.

the two major components which are the differential conductance G_{AC} and differential capacitance C.
The admittance Y is obtained from small signal measurement taken on our DUT with variably DC voltages in the dark. From small signal measurement, the determined differential conductance for a given DC bias voltage and differential capacitance contribute to the differential complex conductance (small signal admittance) of the DUT.

At a selected constant frequency f_o, a small sinusoidal signal υ_{AC} of known constant amplitude produced by the function generator, FG is superimposed by a DC voltage which was varied. The amplified signal is then applied to the DUT which was connected in series with an inductive free resistor, R_i of known value which serves as a current monitor. From the current and voltage values measured, the corresponding admittance will be automatically calculated by the software program. Additionally, the DC current is determined by the digital multimeter scanner (section 3.1.4) while for the AC component, the amplitude as well as the phase relation between the current and voltage is determined by the dual phase lock in amplifier (section 3.1.2) or alternatively with the DSO, so that the complex differential conductance (small signal admittance) could be derived. The experimental setup for the small signal admittance measurement is shown in Fig.3.3. below. Both current and voltage are taken by the same device by switching between input channel CH4 and CH5 of the scanner.

In this study, the frequency of the small AC signal, υ_{AC} introduced, was set up to $10.17kHz$, the signal amplitude was 0.05V peak to peak and a 1Ω inductive free resistor (R_i) was chosen. All measuring instruments in the setup are connected by

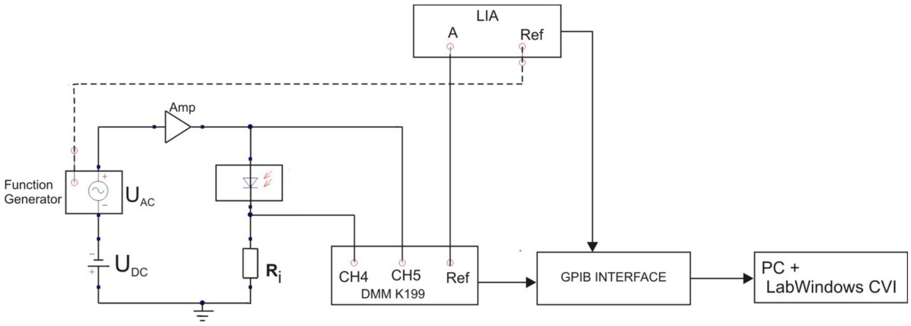

Figure 3.3.: Experimental setup for the small signal measurements.

a GPIB interface to a PC with installed LabWindows CVI software from National Instruments.

3.2.3. Complex impedance measurement

With the same experimental setup of Fig.3.3, the complex impedance can also be measured, that is, "small signal measurement". Here in contrast to the admittance measurements the small AC signal amplitude excited at a series of frequencies is superimposed by a pre-selected DC voltage which was kept constant. The measurements were done in the dark as well as under illumination. Both the phase and the complex impedance as a function of the signal's frequency of the DUT will be automatically calculated by LabWindows CVI software from National Instruments which has been installed on the PC.

In this experimental work, a small AC voltage signal of magnitude 0.05V was generated at frequencies in the range of $14.7Hz$ to $84kHz$ for each selected forward bias voltage. From the real and the imaginary values of the impedance obtained from the small signal measurements, a complex plane plot (impedance spectroscopy) was formed for each bias voltage which was set to: 0.2V, 0.25V, 0.3V, 0.35V, 0.4V, and 0.45V. The results are shown in Fig.4.4, 4.5 and 4.6.

3.2.4. Signal Response Measurement

The sample was exposed to an intensity modulated light. The excitation frequency

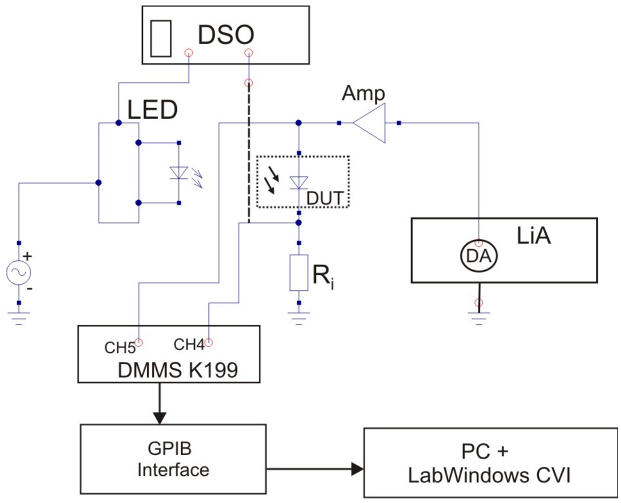

Figure 3.4.: Experimental set up for the signal response measurement.

was varied between $27Hz$ and $100kHz$. The Function generator (sect. 3.1.1) was used to modulate the current of a high power infra red emitting LED. Since the light intensity varies almost linear with the supplied current, the intensity modulation was nearly sinusoidal. The spectral distribution of the emitted light has a peak at $870nm$. The solar cell was biased in the range from -1.4V to +0.3V and the light current was recorded as a function of the frequency.

At the external part of the circuit, the DC voltage bias was introduced in the DUT in series with an inductive free resistance through one of the lock in amplifiers additional digital to analog outputs delivering the DC bias voltage. The output was connected to the power amplifier (3.1.5). As frequency response signal the current caused by the light modulation was measured. An inductive free shunt resistor R_i of 10Ω, or 100Ω was selected to pick up the current.

Finally, the signals, the current through the LED, the light generated current of the DUT were recorded with the oscilloscope and were analyzed by the application of a Fourier-transformation so that the amplitude and the phase of the signal could be evaluated. Both the amplitude and the phase angle of the modulated light current give the frequency response of the solar cell .

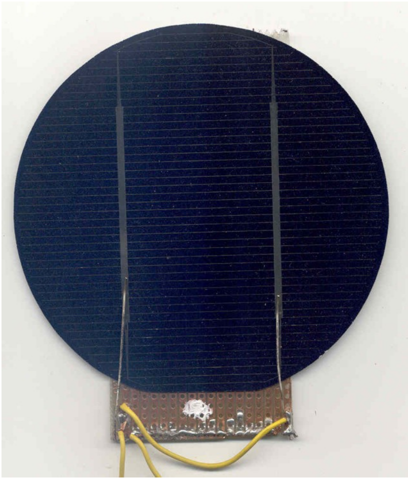

Figure 3.5.: The sample of a p-Si mono crystalline solar cell used in our experiments.

3.3. The sample

In this study, a p-type mono crystalline silicon solar cell of circular shape produced by Tesla with diameter of $99.55mm \pm 0.05mm$, bearing a surface area of $77.84cm^2 \pm 0.04cm^2$ was investigated. The front surface with the metal fingers is shown in Fig.3.5. The surface near n-type region was obtained by phosphorous ion implantation which is best suited to achieve a step gradient at the pn-junction but is less common in solar cell production.

4. Data Evaluation

4.1. Evaluation of the DC Current-Voltage Measurements

In the dark, DC current- voltage measurements were performed. The bias voltage was varied between -2V and +1V. The ambient temperature was 305.7K. In the same voltage range measurements were also done on the illuminated DUT at different intensities. The results are shown in Fig.5.1.

The data were used to evaluate the following parameters of the solar cell:
(1) Static resistance, R_T (Equation 2.17)
(2) Dynamic resistance R_d (Equation 2.18)
(3) Diode saturation currents, I_{01} and I_{02} assuming a 2 diode equivalent circuit (Equation 2.14)
(4) Parasitic resistances R_s and R_{sh}
(5) Solar cell parameter I_{sc} and U_{oc}.

For the data pair fitting, a two diodes model was applied to evaluate the basic diode's parameters like the parasitic resistances (series resistance, R_s and shunt resistance, R_{sh}), diffusion saturation current, I_{o1} and recombination saturation current, I_{o2} based on Equation 2.14. The parasitic resistance values obtained from the data pair fitting are $R_s = 0.072\Omega$ and $R_{sh} = {}^{1}/_{G_{Sh}} = 727.3\Omega$.
Under illumination, the short circuit current, I_{sc} corresponding to the selected intensity level was deduced from the $I(U)$ curve at a bias voltage equal to zero on the vertical axises. With respect to the magnitudes of the parasitic resistances the photo current can be approximated by $I_{ph} \simeq I_{sc}$. Similar to the short circuit current, the voltage maximum for each intensity level is the open circuit voltage, U_{oc} and can also be deduced from the $I(U)$ curve at $I = 0A$ on the horizontal axises. The results are summarized in Table 5.1 and Table 5.2.

4.2. Evaluation of the small signal admittance Measurements

The small signal admittance of the photovoltaic device was evaluated from the differential conductance, G_o and the differential capacitance, C obtained from small signal measurements in the dark and under illumination. Both components vary strongly with the applied bias voltage. According to the small signal assumptions, the admittance, Y_{AC} for each bias voltage is calculated from the linear combination of the real and imaginary component of the AC conductance as given by Equation 2.48 in section 2.3.2.3. The magnitude is given by:

$$Y_{AC} = \mid G_o - iB \mid = \sqrt{G_o^2 + (2\pi f_o C)^2} \tag{4.1}$$

where $f_o = 10.17kHz$ is the selected frequency. The small AC signal was excited with an amplitude of $0.05V_{SS}$.

In subsection 2.3.2.2 the total capacitance, C of a mono crystalline silicon solar cell is derived from the sum of the two voltage dependent components, the depletion capacitance dominating the total capacitance in the reverse bias regime and the diffusion capacitance which is predominant under applied forward bias. In Fig.4.2a the total capacitance is plotted against the applied voltage as obtained from the small signal measurements in the dark and under illumination. The total capacitance is responsible for the small signal AC response of the mono crystalline silicon solar in the dark and under illumination.

With respect to the abrupt junction profile Equation 2.29 in subsection 2.3.2.2, describes the dependence of the junction capacitance in the reverse bias regime. Under this condition the junction capacitance is given by the depletion term, C_{depl} only. The two variables, U_{bi} and N_A, the device specific built-in voltage and acceptor concentration can therefore be derived from the measurement. This can be done graphically by plotting $\frac{1}{C_{depl}^2}$ against the bias voltage U as shown in Fig.4.2b which should follow a linear relation for voltages $U < 0$:

$$\frac{1}{C_{depl}^2} = \frac{-2}{q\epsilon_s\epsilon_o A^2 N_A} U + \frac{2U_{bi}}{q\epsilon_s\epsilon_o A^2 N_A} \tag{4.2}$$

Thus by plotting the experimental data $\frac{1}{C^2_{depl}}$ vrs. U, a linear fit is used to derive these parameters according to:

$$y(x) = mx + d \tag{4.3}$$

Where,

$$m = -\frac{2}{q\epsilon_s\epsilon_o A^2 N_A} \; is\, the\ slope$$

and

$$d = \frac{2U_{bi}}{q\epsilon_s\epsilon_o A^2 N_A} \; is\, the\ intercept$$

Therefore, the doping concentration (acceptor concentration in the base of the cell) N_A was evaluated from the slope for the cell area $A = 77.84cm^2$:

$$N_A = \frac{2}{q\epsilon_s\epsilon_o A^2 m}$$

The built-in voltage, U_{bi} derived from the fitting according to Equation 4.3 is simply found for the condition

$$0 = mx + d$$

or

$$U_{bi} = -\frac{d}{m}$$

Where, q is the electronic charge, ϵ_s is the dielectric constant of the semiconductor (for mono crystalline silicon$\epsilon_{si} = 11.8$ [14], $\epsilon_o = 8.85 \cdot 10^{-14} Fcm^{-1}$ is the permittivity of free space. The results are summarized in Table 5.3.

4.3. Parameter evaluation from impedance spectroscopy

The complex impedance, Z of our p-type mono crystalline silicon solar cell derived from small signal measurements with varying excitation frequency f consists of the real and the imaginary part. With the real and imaginary magnitude of the impedance, a plot of $(Re(Z) + Im(Z))$ in the complex plane at different bias voltages forms an impedance spectrum as shown in Fig.4.3 from measurements in the dark, in Fig.4.4 for a low incident light intensity, and in Fig.4.5 for a high illumination level. The impedance spectra were taken for a series of forward bias voltages, U_{bias} roughly covering the operating range of the solar cell.
From these experiments the following parameters of interest were derived:

(1) Internal dynamic resistance R_d
(2) Series resistance r_s
(2) Diffusion capacitance C_d
(3) Minority carriers life time τ_p

The evaluation of these parameters was done according to the approach of Suresh [26]. By plotting the cell's impedance obtained from the measurement at varying frequencies, the data pairs $Re(Z)$, $Im(Z)$ follow basically a semicircle in the complex plane as illustrated in Figs. 4.3, 4.4 and 4.5.
The diameter of the semicircle along the real axis represent R_d. The offset from zero as can be seen i.e. in Fig.4.3f is the series resistance, r_s. C_d and the corresponding frequency, f_{max} is derived for the condition $Im(Z) = max$:

$$C_d = \frac{1}{2\pi f_{max}(Im(Z))_{max}} = \frac{1}{2\pi f_{max} X_C} \tag{4.4}$$

From C_d and R_d , τ_p is calculated:

$$\tau_p = \frac{R_d C_d}{2} \tag{4.5}$$

The results of the evaluation is summarized in Table 5.4, 5.5 and 5.6.

4.4. Evaluation of signal response measurements

The block diagram of the setup for the determination of the cell's signal response is given in Fig.3.4. The AC signal across the external resistor, R_i was analyzed with respect to the amplitude as well as the phase shift of the first harmonic. The cutoff frequency, f_{RC} for each bias voltage was deduced at 70.07% attenuation of the amplitude of the signal. The internal resistance, R_d together with the externally connected resistor, R_i are the real branch of the current divider that causes the observed differences of f_{RC} when using either $R_i = 10\Omega$ or $R_i = 100\Omega$ as shown in Fig.4.7.

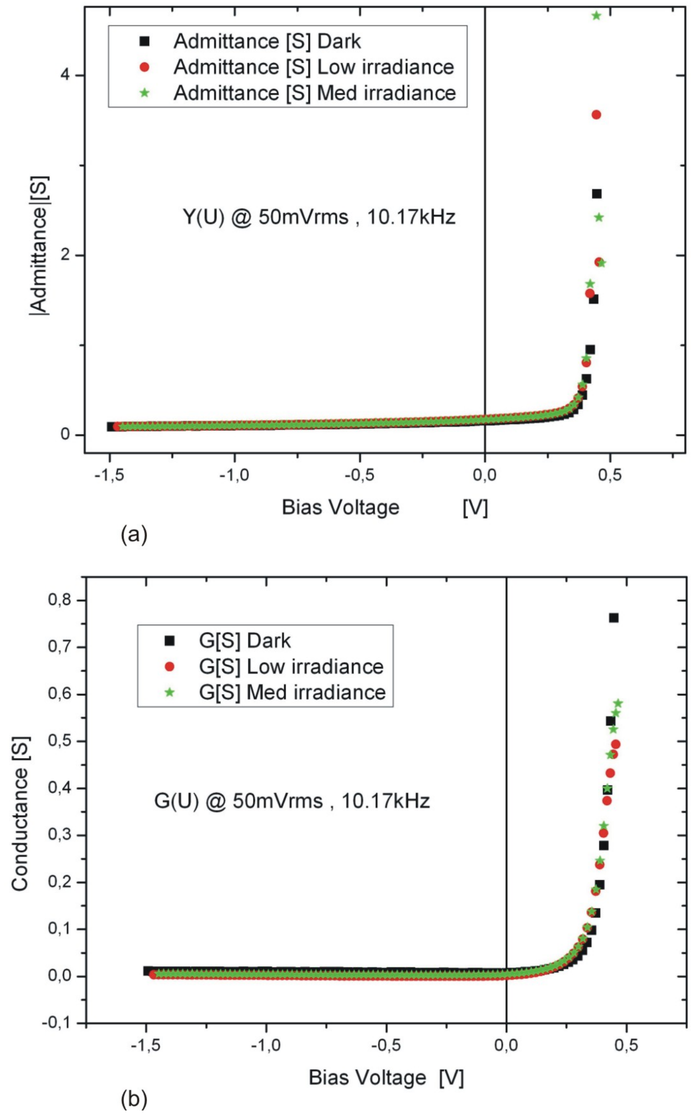

Figure 4.1.: (a): Evaluated solar cell admittance in the dark and under illumination as a function of the bias voltage.
(b): Differential conductance of the cell in dark and under illumination obtained from small signal measurements as a function of the bias voltage.

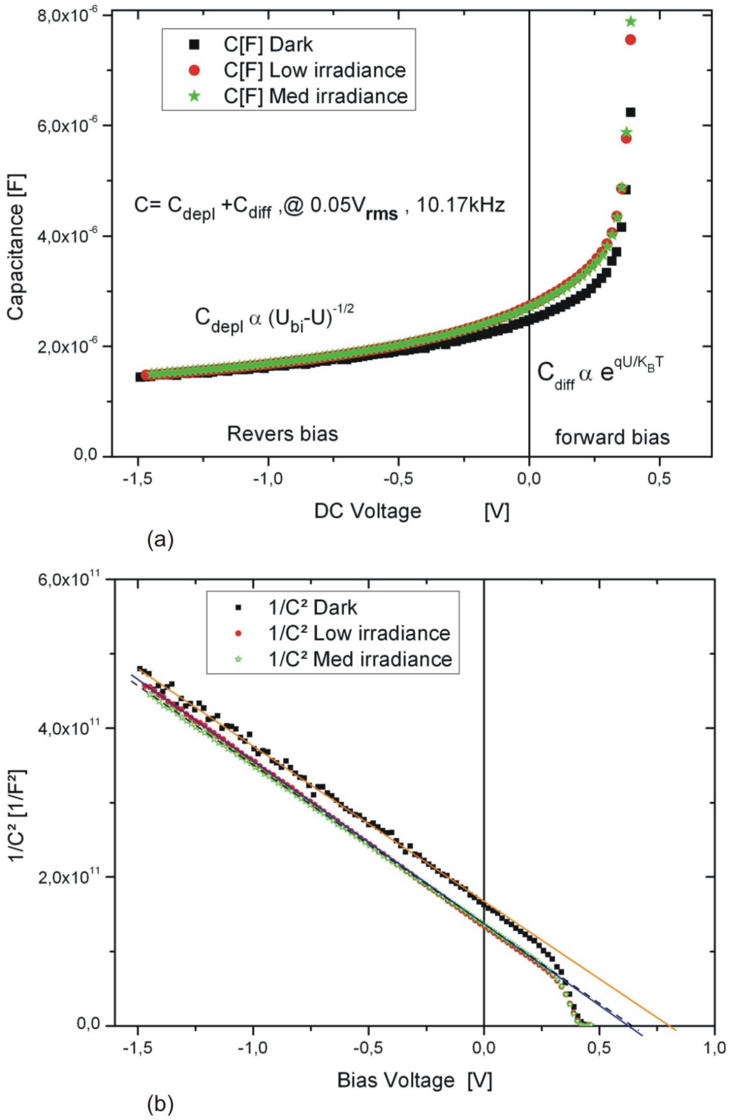

Figure 4.2.: (a): Capacitance-voltage characteristics of the solar cell in the dark and under illumination achieved from small signal admittance measurements.
(b): Evaluation of the built in voltage and the doping concentration from a linear data fit of the cell capacitance in the dark and under illumination.

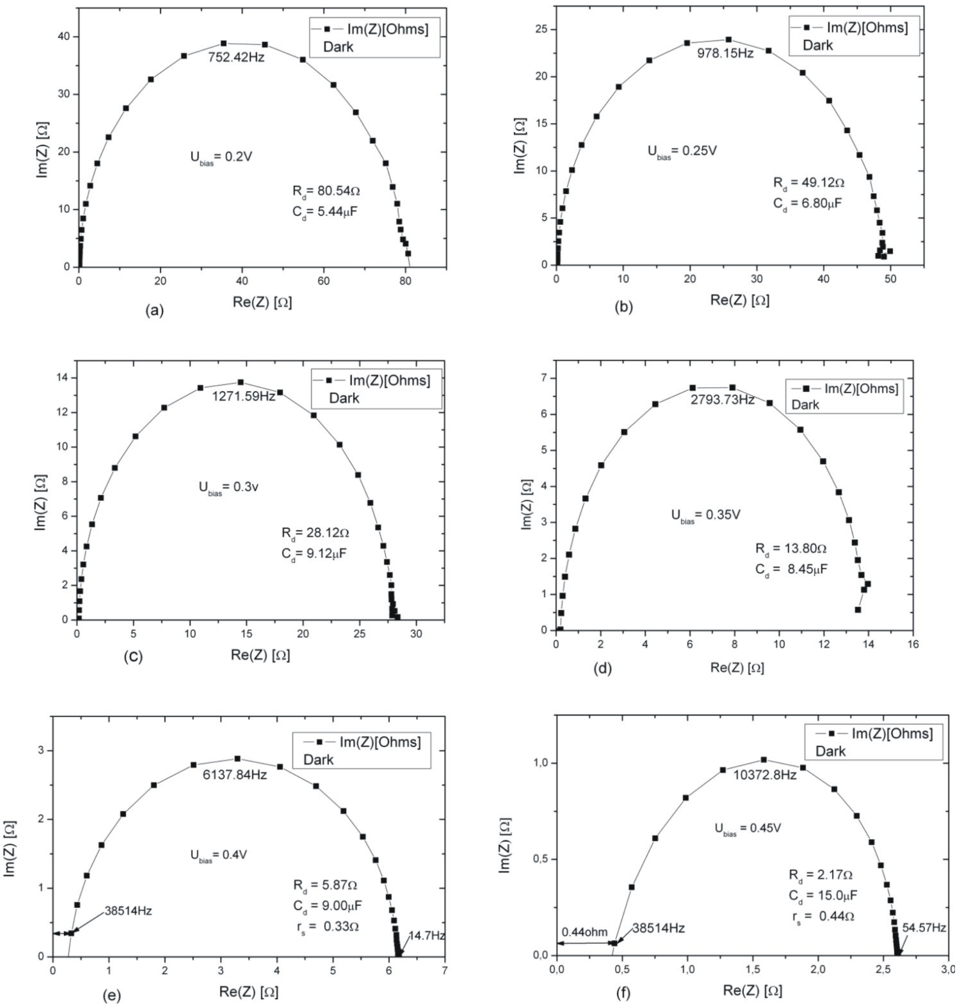

Figure 4.3.: Impedance spectrum of the p-Si solar cell achieved for different forward bias voltages (a) through (f) in the dark. The according bias voltage is shown in the Fig.

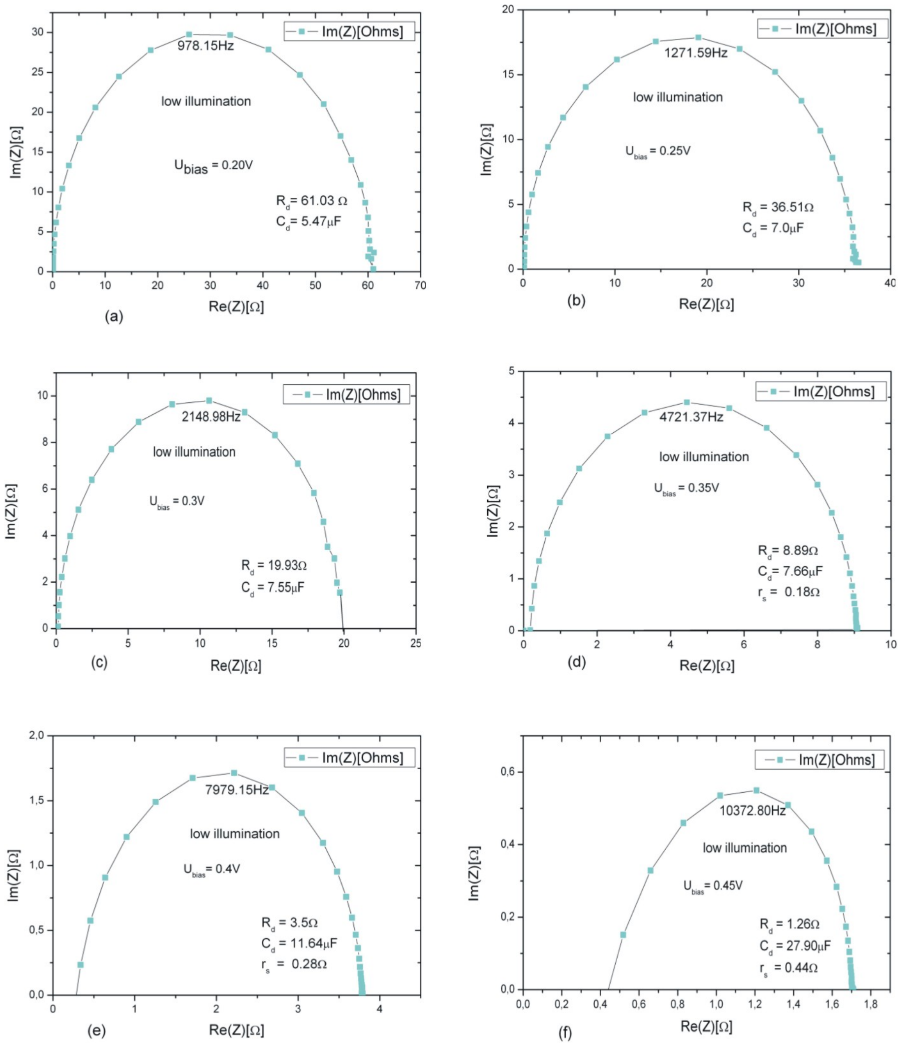

Figure 4.4.: Impedance spectra under low illumination. All other conditions are unchanged.

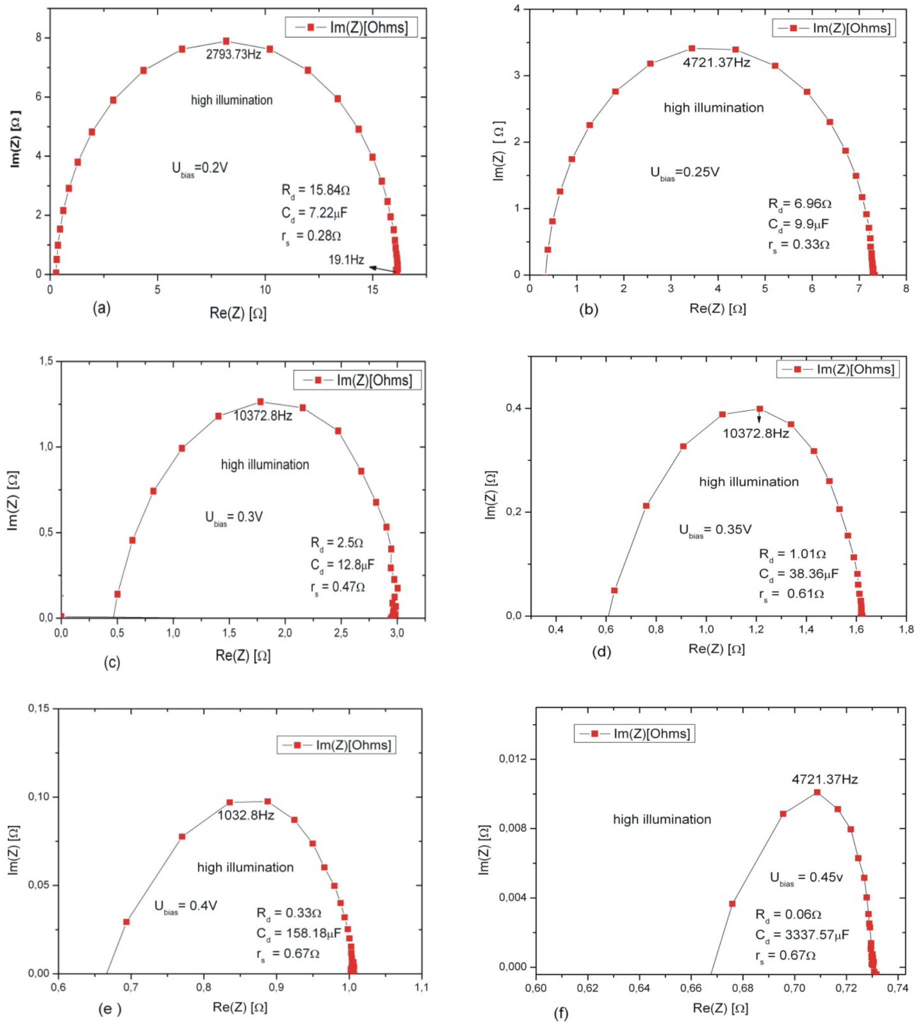

Figure 4.5.: Impedance spectrum observed under high illumination. All other conditions are unchanged.

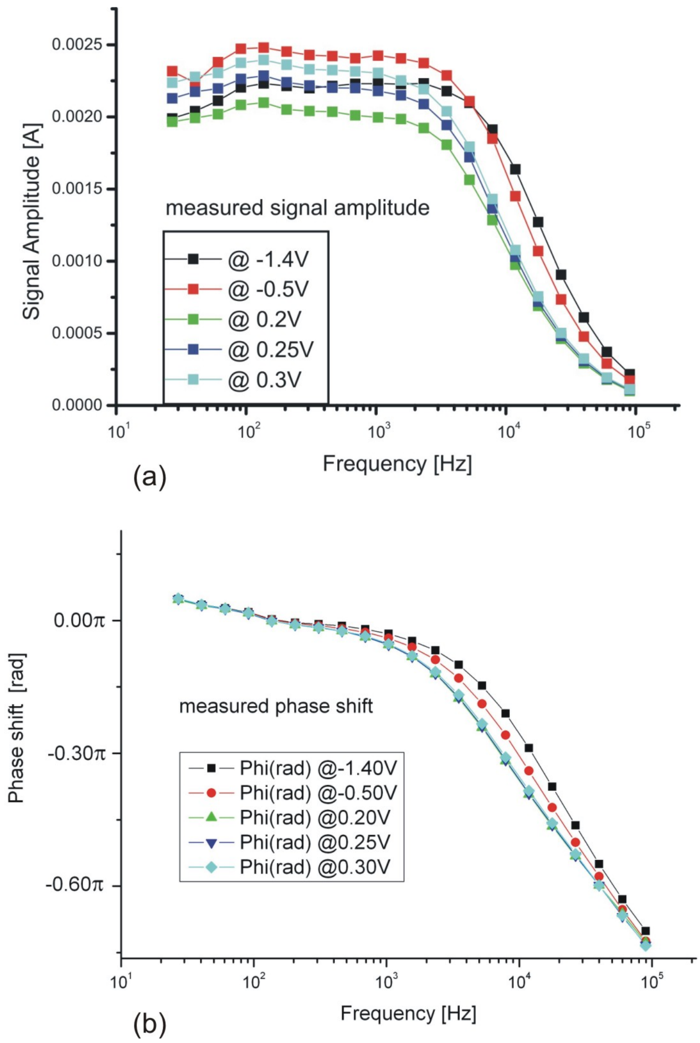

Figure 4.6.: (a) shows the resulting signal amplitudes of the light induced AC current for five bias voltages. The corresponding phase shifts are shown in (b)

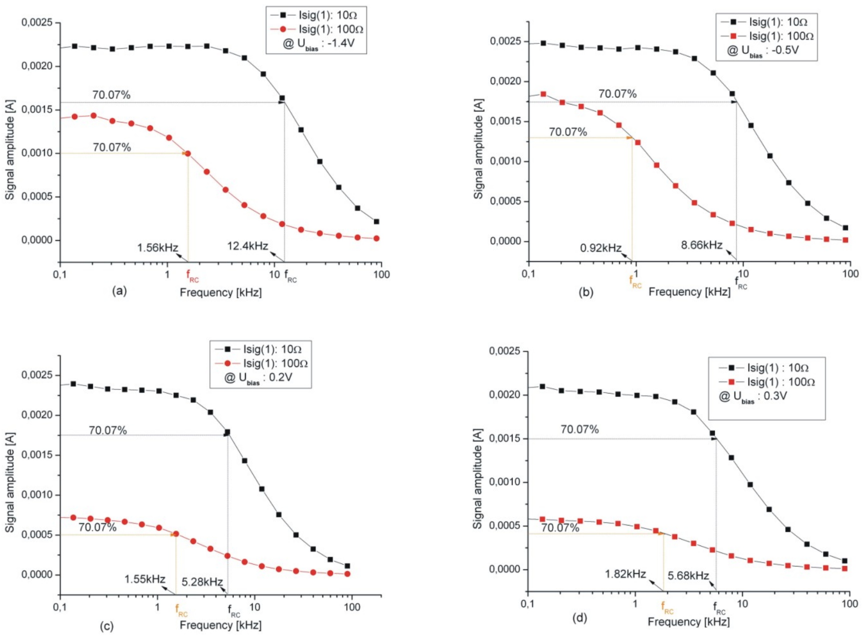

Figure 4.7.: The influence of the external resistor $R_i$on the cut off frequency f_{RC} is shown for the reverse biased cell (a and b) and for the forward biased cell (c and d).

5. Results and Discussion

DC measurements and AC measurements were made in the dark and under illumination for a p-type mono crystalline silicon solar cell with an area of $77.84cm^2$. From the measurements the cell's admittance and conductance as a function of the applied voltage was derived as shown in Fig.4.1. The DC parameters of the cell were determined and are summarized in Table 5.1.

From initial DC measurements performed in the dark, the diode parameters like saturation current and the parasitic resistances R_s& R_{sh} were evaluated assuming an internal circuit with two diodes. A least square fit of the measured $I(U)$ data to the model was performed. This procedure was repeated for different illumination intensities, from which the light current ($I_{ph} \simeq I_{sc}$) as well as the open circuit voltage (U_{oc}) for each level of intensity of were determined (Table 5.2).

Small signal measurements were performed in the dark and under illumination at a pre set constant frequency of $10.17kHz$ in order to derived the AC admittance as well as the junction capacitance of the DUT as a function of the bias voltage The results are shown in Fig.4.1 and Fig.4.2a. A linearization of the squared reciprocal capacitance as a function of the applied voltage in the reverse bias regime was used to evaluate the built-in voltage and the doping concentration of the cell's step-like pn-junction (Table 5.3). From the impedance spectra achieved from small signal measurements at varying excitation frequencies, the AC parameters: C_d, R_d, and τ_p were evaluated for a series of constant forward bias voltages, U_{bias}. This was done as well for experiments in the dark (Table 5.4) as under illumination (Table 5.5and 5.6).

Finally, the analysis of the signal response of the DUT was elaborated. It was based on the measurements of the cell's AC current introduced by a sinusoidally intensity modulated light with variable frequency. Both, amplitude attenuation

Parameter	Value
Series resistance R_s	0.072Ω
Shunt resistance R_{sh}	727.30Ω
Static resistance R_T	3.0Ω
Dynamic resistance R_d	0.23Ω
Recombination saturation current I_{o2}	$6.25\mu A$

Table 5.1.: Evaluated cell parameters of a mono crystalline silicon solar cell with an area $A = 77.84cm^2$ deduced from the DC I-U curve in the dark.

Illumination level	Short circuit current I_{sc} $[A]$	Open circuit voltage U_{oc} $[V]$
low	0.04	0.46
medium	0.12	0.49
high	0.29	0.50
very high	0.55	0.50

Table 5.2.: Short circuit current and open circuit voltage deduced from I-U curves under illumination.

and phase shift were analyzed. Also from the amplitude attenuation to 70.17% of it's original value the cutoff frequency, f_{RC} of the device was extracted for several bias voltages (Table 5.7).

From the plot $I(U)$ shown in Fig.5.1, it was observed that the short circuit current varies linearly with the incident intensity which is in agreement with the current-voltage characteristic expressed by Equation 2.10. The open circuit voltage however shows only a slight variation with the intensity. According to Equation 2.8 U_{oc} shall depend on I_{sc} and therefore on the intensity in a logarithmic manner. In the case of the dark $I(U)$ curve, it was observed that the recombination saturation current dominates over the diffusion term once a two diode model for the data pair

State	Doping concentration N_A $[cm^{-3}]$	Built in voltage $U_{bi}[V]$
Dark	$1.0 \cdot 10^{16}$	0.82 ± 0.01
low illumination	$0.90 \cdot 10^{16}$	0.60 ± 0.01
medium illumination	$0.94 \cdot 10^{16}$	0.64 ± 0.03

Table 5.3.: Summary of the results of the pn-junction analysis in the dark and under illumination.

U_{bias} $[V]$	C_d $[\mu F]$	@ f_{max} $[Hz]$	$R_d[\Omega]$	r_s $[\Omega]$	τ_p $[\mu s]$
+0.20	5.44	752.42	80.54	-	219.07
+0.25	6.80	978.15	49.12	-	167.00
+0.30	9.12	1271.59	28.12	-	128.23
+0.35	8.45	2793.73	13.80	-	58.31
+0.40	9.00	6137.84	5.87	0.33	26.42
+0.45	15.00	10372.80	2.17	0.44	16.28

Table 5.4.: AC parameters derived from impedance spectrum analysis in the dark.

fitting was applied.

According to the static $I(U)$ curve from the in Fig.5.1 from the experiment, we consider the effect of external voltage U on a pn-junction solar cell under illumination condition with respect to forward bias regime $U > 0$ (section 2.2.1). Since for U_{oc} the net current is zero the internal voltage at the diode, U' equals the experimentally observed external voltage U_{oc} (Equation 2.9).

The values of the diffusion capacitance, C_d and internal dynamic resistance, R_d of the cell together with the known value of the externally used resistor, $R_i$were used to calculate the cut off frequency under forward voltage conditions (Equation 2.62). The calculated values of f_{RC} were compared with the results of the signal response measurements and are shown in Fig.5.2. Solid lines represent the calculation whereas symbols indicate the experimental findings. A poor agreement can be seen which may be caused by several reasons which were not investigated further within this work.

A plot of the minority carrier lifetime, τ_p derived from the impedance spectra versus the applied forward voltage in Fig.5.3 shows a variation over one decade and considerably changes with the incident light intensity. This is in contrast to the assumed constant value for τ used in Equation 2.30 and Equation 2.31. Both Equations however are approximations for either low or high frequencies

$U_{bias}\,[V]$	$C_d\,[\mu F]$	$@f_{max}\,[Hz]$	$R_d\,[\Omega]$	$r_s\,[\Omega]$	$\tau_p\,[\mu s]$
+0.20	5.47	978.15	61.03	-	166.92
+0.25	7.00	1271.59	36.51	-	127.79
+0.30	7.55	2148.98	19.93	-	75.24
+0.35	7.66	4721.37	8.89	0.18	34.49
+0.40	11.64	7979.15	3.50	0.28	20.37
+0.45	27.90	10372.80	1.26	0.44	17.58

Table 5.5.: AC parameters deduced from impedance spectrum analysis under medium illumination.

$U_{bias}\,[V]$	$C_d\,[\mu F]$	$@\,f_{max}\,[Hz]$	$R_d\,[\Omega]$	$r_s\,[\Omega]$	$\tau_p\,[\mu s]$
+0.20	7.22	2793.73	15.84	0.28	57.18
+0.25	9.90	4721.37	6.96	0.33	34.45
+0.30	12.80	10372.80	2.50	0.47	16.00
+0.35	38.36	10372.80	1.01	0.61	19.37
+0.40	158.18	1032.80	0.33	0.67	26.10
+0.45	3337.57	4721.37	0.06	0.67	100.13

Table 5.6.: AC values deduced from impedance spectrum analysis for very high illumination.

($\omega\tau \ll 1$ or $\omega\tau \gg 1$). The observed behavior suggests that the experimentally accessed frequency range is somewhere in between. For instance taking values for $f_{max} = 1272Hz$ and $\tau_p = 128\mu s$ for a bias voltage of 0.25V from Table 5.5 result in $2\pi f_{max}\tau_p = 1.02$ which confirm this suspicion. Towards higher bias voltages ($U \geq 0.45V$) τ_p has the tendency to approach a constant value of about $15\mu s$.

Cut off freq f_{RC} $[kHz]$	@ $U_{bias}[V]$
12.40	-1.40
8.66	-0.50
5.28	+0.20
5.68	+0.30

(a)

Cut off freq f_{RC} $[kHz]$	@ $U_{bias}[V]$
1.56	-1.40
0.95	-0.50
1.55	+0.20
1.82	+0.30

at

(b)

Table 5.7.: Table (a) shows the cutoff frequency found from signal response measurements using a shunt resistor, $R_i = 10\Omega$ while table (b) shows the cutoff frequency when $R_i = 100\Omega$.

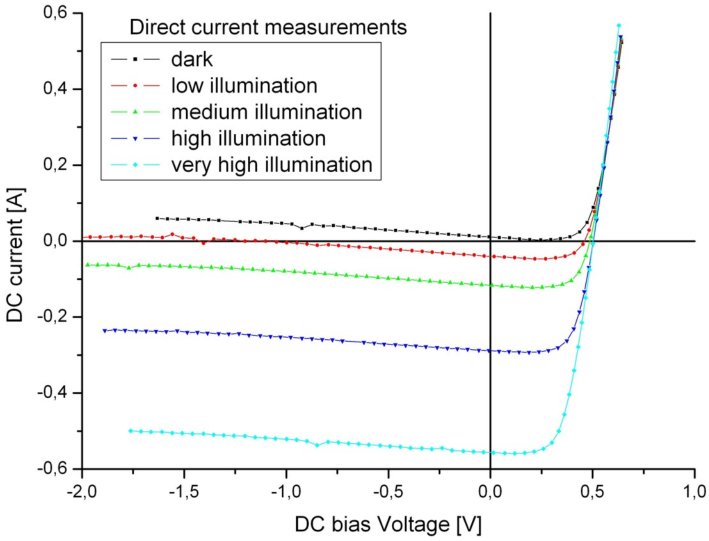

Figure 5.1.: Current-voltage characteristic of a p-type mono crystalline silicon solar cell obtained from measurements in the dark and under illumination with varying intensity.

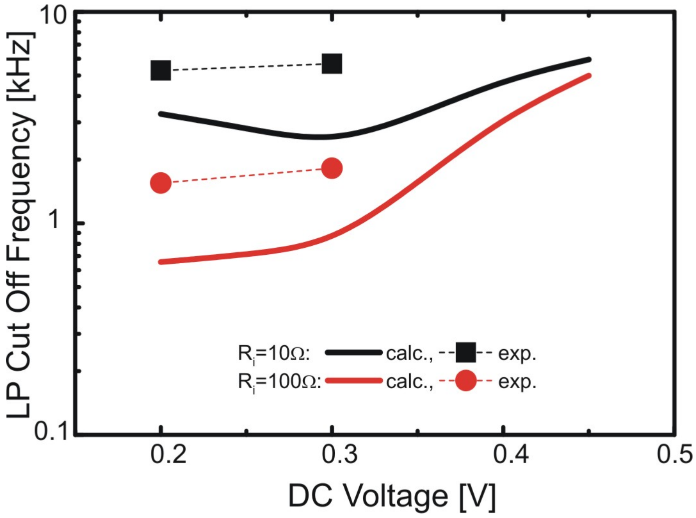

Figure 5.2.: Comparison of the calculated and experimentally determined Low-Pass cut off frequency under forward bias conditions.

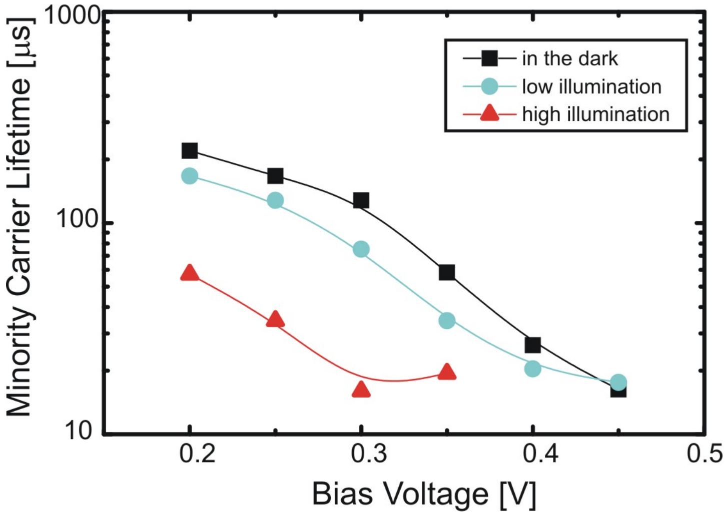

Figure 5.3.: Minority carrier life time as a function of the applied bias voltage for different light intensities.

6. Conclusions

The complex impedance of a mono crystalline silicon solar cell exposed to light was experimentally investigated in the frequency range between $10Hz$ and $500kHz$ and analyzed with the help of an appropriate equivalent circuit model. The implicit Low Pass characteristic of this model could be experimentally confirmed. However the attempt to interpret the components of the assumed circuit by semiconductor physics was insufficient. This was partially caused by experimental limitations which inhibit to accurately maintain certain boundary conditions. An influence of the illumination intensity on the AC parameters of photovoltaic device was observed. Among the cell parameters, the diffusion capacitance varies with respect to the forward bias voltage in agreement with theory. Basically it increases exponentially with voltage. As a consequence the cut off frequency, f_{RC} of the Low Pass filter increases towards higher voltages. Since data acquisition for quality tests in the photovoltaic industry covers the range between $U = 0V$ and $U = U_{oc}$ the error introduced by a high sampling rate will be larger around short circuit current conditions and decrease towards the open circuit voltage. For the investigated cell a sampling rate of 5kSa/s might be appropriate around U_{oc} for an error of 1 per cent or less but may introduce an error of more than 20 per cent at $U \sim 0V$.
Finally, it can also be said that photovoltaic solar cells show DC and AC behavior, which are easily distinguishable in terms of the used circuit model. That means, that the DC model can be extended to analyze the complex impedance of the solar cell.

The data for $I(U)$ curves collected at very fast sampling rates (i.e $>$ 1kSa/s) will not match with that of the static case, because there will be deviation in the data recording as a result of the condition on which the measurements were done. In the static case the data recording time is selected sufficiently long enough for every step that the device can settle to the selected working point. In the dynamic case the short interval between successive data acquisition does not allow the device to completely settle at the working point. Therefore the sampling rate has to be carefully evaluated in order to keep the recorded data within tolerable error limits.

References

1. A.Goetzberger V.U. Hoffmann, “Photovoltaic Solar Energy Generation”, Springer Series in Optical Sciences 112, 2005.
2. H.G. Wagemann, H. Eschrich “Grundlagen der photovoltaischen Energiewandlung”; Teubner Verlag, Stuttgart 1994.
3. J. Nelson. “The physics of solar cells”, Imperial College Press, London, 2003.
4. A. Luque, S. Hegedus, “Handbook of Phovoltaic Science and Engineering”, John Wiley and Sons, 2003.
5. R. F. Pierret, “Semiconductor Device Fundamentals”, 1st Ed., Addison Wesley Longman, 1996, p.216-305.
6. J.S. Yuan and J. J. Liou, “Semiconductor Device Physics and Simulation”, Springer Verlag, 1998, p.35-37.
7. M L Lucia, J L Hernandez-Rojas, C Leon and I Mártil, “Capacitance measurements of p-n junctions: depletion layer and diffusion contributions”, Eur. J. Phys. **14** 86, 1993, p. 86-89, (doi: 10.1088/0143-0807/14/2/009).
8. R. Müller, “Grundlagen der Halbleiter-Elektronik”, Springer Verlag, Berlin, Heidelberg, New York, 1971, p.128-132.
9. J. Millman, C.C. Halkias, “Integrated Electronics: Analog and Digital Circuits and Systems”, McGraw-Hill, New York, 1972.
10. N. W. Ashcroft, N. D. Mermin, “Solid State Physics”, Holt, Rinehart and Winston, 1976.
11. S. Krishnamurthy, “Solar and fuel cell circuit modelling, analysis and integrations with power conversion circuit for distributed generation”, Thesis, University of Central Florida, Orlando, Florida, 2009.
12. V. Schlosser, A. Ghitas, “Measurement of silicon solar cells ac parameters”, Proc.of the Arab Regional Solar Energy Conference (Manama, Bahrain, 2006).
13. E. Kanscár, “ Measurement and simulation of cell alternating current parameters, Diploma Thesis, University of Vienna, 2010.

14. B. G. Streetman, S. Banerjee, " Solid State Electronic Devices", 6^{th}Ed., Prentice Hall, 2005.
15. D. Chenvidhya, K. Kirtikara, C. Jivacate, "A new characterization method for solar cell dynamic impedance", Solar Energy Materials & Solar Cells, **80**, 2003, p.459-464.
16. S. Mau, T. Krametz, "Influence of solar cell capacitance on the measurement of IV curves of PV modules", Proc. 20^{th} ECPVSEC (Barcelona, 2005), p.2175-2177.
17. M. P. Deshmukh, J. Nagaraju, "Measurement of $CuInSe_2$ solar cell AC parameters", Solar Energy Materials & Solar Cells, **85**, 2005, p.407-413.
18. Z. Ounnoughi, M. Chegaar, "A simpler method for extracting solar cell parameters using the conductance method", Solid-State Electronics, **43**, 1999, 1985-1988
19. S. Kumar, P. K. Singh, G. S. Chilana, "Study of silicon solar cell at different intensities of illumination and wavelengths using impedance spectroscopy", Solar Energy Materials & Solar Cells, **93**, 2009, 1881-1884 (doi:10.1016/j.solmat.2009.07.002).
20. W. Demtröder, "Experimentalphysik 2 (Elektrizität und Optik)", Springer-Verlag, Berlin Heidelberg, 1999.
21. B. Wilson, "Depletion Width", The Connexions Project, module: m1006, published under http://cnx.org/content/m1006/2.16/
22. J.-P. Charles, I. Mekkaoui-Alaoui, G. Bordure, P. Mialhe, "Etude comparative des modèles à une et deux exponentielles en vue d'une simulation précise des photopiles", Rev. Phys. Appl. (Paris) **19**, 1984, p.851-857 (doi: 10.1051/rphysap:01984001909085100).
23. G.L. Araujo, E. Sanchez and P. Marti, "Determination of the two-exponential solar cell equation parameters from empirical data", Solar Cells, **5**, 1982, p. 199-204,
(doi:10.1016/0379-6787(82)90027-8).
24. Wikipedia contributors, "Low-pass filter" Wikipedia, The Free Encyclopedia, http://en.wikipedia.org/w/index.php?title=Low-pass_filter&oldid=435007869 (accessed July 1, 2011).
25. Florida Solar Energy Center, "Photovoltaic Info" accessible under: http://www.schroederssolar.com/resources/photovoltaicinfo.pdf

26. M. S. Suresh, "Measurement of solar cell parameters using impedance spectroscopy", Solar Energy Materials & Solar Cells, **43**, 1996, p.21-28 (doi:10.1016/0927-0248(95)00153-0).
27. S. M. Sze, "Semiconductor Devices Physics and Technology", John Wiley & Sons, New York, 1985, p.16-20.

A. Appendix

A.1. List of symbols

Symbol	Name	Units
A	junction area	cm^2
U	DC bias voltage	V
U_{bi}	built in voltage	V
U_{oc}	open circuit voltage	V
υ_{AC}	alternating voltage	V
υ_o	small signal voltage amplitude	V
I_{diff}	diffusion current	A
J	current density	A/cm^2
I_{o1}	diffusion saturation current	A
I_{o2}	recombination saturation current	A
i_{AC}	alternating current	A
I_{sc}	short circuit current	A
C_{depl}	depletion capacitance	F
C_{diff}	diffusion capacitance	F
G_o	differential conductance	S
G_{sh}	shunt conductance	S
Y	complex admittance	S
Z	impedance	Ω
T	temperature	K
N_A	acceptor concentration	$number\ acceptors/cm^3$
N_D	donor concentration	$number\ donors/cm^3$
W	junction width	μm
R_s	series resistance	Ω
R_{sh}	shunt resistance	Ω
R_T	static resistance	Ω
R_d	dynamic resistance	Ω
X_L	inductive reactance	Ω
X_C	capacitive reactance	Ω

Symbol	Name	Units
f_o	signal frequency	Hz
f_{RC}	Cut off frequency	Hz
ω	angular frequency	rad/s
τ_p	minority carrier life time	sec
τ_{SCR}	carrier life time in the space charge region	sec
B	susceptance	S
E_F	Fermi level	eV
E_g	energy band gap	eV
E_{vac}	vacuum level	eV
E_i	intrinsic energy level	eV
E_c	conduction band edge	eV
E_v	valence band edge	eV
n_i	intrinsic carrier concentration	cm^{-3}
n_o	equilibrium concentration of electrons	cm^{-3}
p_o	equilibrium concentration of holes	cm^{-3}
p_n	hole concentration at depletion edge	cm^{-3}
n_p	electron concentration at depletion edge	cm^{-3}
Φ_n	work function of an n-type semiconductor material	eV
Φ_p	work function of a p-type semiconductor material	eV
P	power	W
P_{max}	maximum power	W
I_{max}	maximum current	A
U_{max}	maximum voltage	V
U_T	thermal voltage	mV or V
G_P	power gain	dB
G_U	voltage gain	dB
G_I	current gain	dB
X_L	inductive reactance	Ω
X_C	capacitive reactance	Ω
ϵ_s	relative dielectric constant	_
ϵ_o	permittivity of free space	F/cm

A.2. Constants

Symbol	Name	Value	Units
q	electronic charge	$1.602 \cdot 10^{-19}$	C
ϵ_o	permittivity of a free space	$8.85 \cdot 10^{12}$	F/cm
ϵ_{si}	dielectric constant of silicon	11.8	_
K_B	Boltzmann constant	$8.617 \cdot 10^{-5}$	eV/K

B. Curriculum vitae

Name:	Ebe Henry Ugochukwu B.Tech.(Physics)
Date of birth:	October 29th 1974
Place of birth:	Imo State, Nigeria.
Nationality:	Nigeria
Status:	Single
Address:	Türkenstrasse 23/2/14, A-1090, Wien.
E-mail:	ebe_henry@yahoo.com
Telephone:	0664 6357 637
Diploma Thesis :	Investigations of the complex impedance of Photovoltaic cells under illumination. Supervisor: Ass. Prof. Dr. Viktor Schlosser
1981-1987:	Constitution Chrisent Primary School Aba, Abia State, Nigeria.
1987-1990:	Queen of the Apostle Secondary Technical School Okigwe, Imo State ,Nigeria
1991-1993:	Community Secondary School Ikenanzizi Obowo L.G.A, Imo State Nigeria.
1993-1994:	Community Secondary School Emekuku, Owerri, Imo State, Nigeria.
May/June.1994:	Senior Secondary School Certificate Exame (S.S.C.E) .
1997-2001:	B.Tech Physics in Faculty of Science, Federal University of Technology Owerri, Imo State, Nigeria.
April.2002-2003:	German course in Vienna
Oct.2004- present:	Studies in Physics at the Faculty of Science, University of Vienna, Austria.

C. - Abstract - English

This paper presents the study of the AC behavior of a photovoltaic device under low and high illumination operated at different DC forward bias voltages. A small signal sinusoidal wave experiment was used for the investigations. The impedance spectra for each illumination level were derived at excitation frequencies ranging from 14.7Hz up to 84kHz and compared with that derived in the dark. For the investigated crystalline silicon solar cell it was observed that the electrical parameters vary with the rise in intensity of illumination as well as with the frequency. From the impedance spectra for each DC forward bias, the cell diffusion capacitance, dynamic resistance and mean carrier life time were calculated. Similarly, other cell parameters (doping concentration and built in voltage) were determined from the capacitance-voltage relation found by the small signal admittance measurements.

Additionally, the DC current-voltage characteristic for both dark and illumination were derived from DC measurements from which other cell DC parameters (shunt resistance, series resistance, saturation current etc) were deduced.

Finally, the low pass filter characteristic of the device was also investigated by determining the signal response (frequency response) of the photo-current caused by the intensity modulation of the incident light.

Key words: Photovoltaic cell, Cell parameters, frequency dependence

D. - Abstract- German

In dieser Arbeit wurde das Wechselstromverhalten eines beleuchteten Photovoltaikelements untersucht. Dazu wurde die Solarzelle bei verschiedenen Lichtintensitäten im elektrischen Durchlaßbereich vermessen. Zur Bestimmung der interessierenden Wechselstromgrössen wurden Kleinsignalexperimente mit einer sinusförmigen Spannung ausgeführt. Die Impedanzspektren für jede Lichtintensität wurden aus den Messungen im Frequenzbereich zwischen 14.7Hz und 84kHz abgeleitet und mit den Ergebnissen für die unbeleuchtete Zelle verglichen. Für die untersuchte Solarzelle aus kristallinem Silizium konnte eine Veränderung der elektrischen Parameter sowohl bei steigender Intensität des einfallenden Lichts als auch bei der Variation der Anregungsfrequenz beobachtet werden. Von den ermittelten Impedanzspektren bei jeder der konstant gehaltenen Zellspannungen wurde die Diffusionskapazität, der dynamische Widerstand und die mittlere Lebensdauer der Ladungsträger berechnet. Weiters wurde die Dotierungskonzentration und die Diffusionsspannung aus dem Zusammenhang zwischen Kapazität und Spannung bestimmt.

In Ergänzung wurden die Strom- Spannungskurven im Gleichstromfall für die unbeleuchtete und beleuchtete Zelle gemessen und daraus die Gleichstromparameter: Parallel- und Serienwiderstand, Sättigungsstrom, abgeleitet.

Abschliessend wurde die Tiefpass-charakteristik des lichtgenerierten Zellenstroms bei intensitätsmodulierter Beleuchtung untersucht.

Key words: Photovoltaische Solarzelle, Solarzellenparameter, Frequenzabhängigkeit.